Journal of Computational Applied Mechanics 2024, 55(4): 783-811

DOI: 10.22059/jcamech.2024.376719.1100

REVIEW PAPER

Exploring the filtration mechanisms in spiral microchannels: A critical review in inertial microfluidics

Mitra Akhbari, Mohsen Nasr Esfahany*

Department of Chemical Engineering, Isfahan University of Technology, Isfahan, 8415683111, Iran

Abstract

A crucial aspect in the design of spiral microchannels is understanding the equilibrium position of particles within them. With a wide array of applications in biomedicine and industry, numerous studies have been carried out to investigate the physical mechanisms influencing particle equilibrium, such as inertial lift and Dean drag forces. Past research, comprising various independent case studies, has highlighted that conventional spiral designs struggle to control lift forces, whereas enhancing the spiral microchannel design can regulate Dean flow intensity effectively. However, there remains a pressing need to delve deeper into and elucidate this phenomenon. This review article systematically concentrates on the factors that influence the shape and intensity of Dean vortices across the cross-section, ultimately determining the particles' equilibrium position within these systems. By synthesizing findings from both experimental and numerical approaches, the study investigates the key factors that govern particle equilibrium positions. Furthermore, the importance of shaping and positioning Dean vortices to effectively manipulate particle trajectories within spiral microchannels is emphasized. Additionally, the advantages and limitations of different cross-sectional shapes (rectangular, trapezoidal, complex) and loop patterns within spiral geometries are deliberated upon to enable more precise particle manipulation strategies.

Keywords: Inertial microfluidics; Spiral microchannel; Particle equilibrium position; Dean flow.

1. Introduction

The manipulation of micrometer-sized particles is crucial in various scientific fields [1], including life sciences, chemistry, and material sciences [2], as well as drug discovery [3]. Conventional separation methods like filtration and centrifugation have limitations such as clogging and high costs [4, 5]. Therefore, there is a need for new techniques that are cost-effective and enable rapid, label-free and trustable particle separation [6, 7].

Microfluidic technology involves the precise control of extremely small amounts of fluids (from 10^{-9} to 10^{-18} L) through the use of channels ranging in size from tens to hundreds of micrometers [8]. Microfluidics, as a rapidly evolving technology, offers numerous compelling benefits over traditional macroscale technology like. These may

* Mohsen Nasr Esfahany. Tel.: +98-311-3391-5631; fax: +98-311-3391-2677.
E-mail address: mnasr@iut.ac.ir

include (1) reduced sample and reagent requirements; (2) shorter analysis times; (3) enhanced detection sensitivity; (4) cost-effectiveness; (5) compact design; and (6) excellent automation and integration features, minimizing the risk of human error [8, 9]. Due to its ability to manipulate small amounts of fluids and its potential to revolutionize biomedicine and clinical diagnostics, microfluidics is anticipated to be a groundbreaking technology. The precise manipulation of particles, such as cells, is crucial in many biological assays, medical diagnostics, and environmental purposes [10, 11]. For instance, in biomedical LOCs, microparticle separators are vital for efficiently separating human T-lymphocytes (CD4+) from whole blood, which is important for diagnosing and treating HIV [12]. Similarly, separating neuroblastoma and glioma cells could be useful for cell replacement therapy in neurodegenerative disorders (e.g., Parkinson's disease, Alzheimer's disease, Multiple sclerosis) and cancer [13, 14]. Furthermore, microparticle separators also find applications in the environmental sector, such as in the extraction of harmful bacteria or metal nanoparticles for water quality analysis. This manipulation is based on variations in the biological and physical traits of the particles, including size, shape, magnetism, dielectric properties, and density [11, 15].

Numerous microfluidic technologies for particle manipulation have been developed, and among them is the inertial microfluidic technique. Inertial microfluidic techniques offer precise fluid control on a microscale, allowing high-throughput manipulation of particles [16, 17]. In these techniques, microchannel geometries play a vital role in influencing particle trajectories [15]. For instance, in straight microchannels, particle focusing is mainly controlled by inertial lift forces. Various cross-section shapes in straight microchannels result in different positions and number of focusing line of particles [18, 19]. Additionally, the varying aspect ratios of the rectangular cross-sectional straight microchannels affect not only the final number of particle equilibrium positions but also the equilibrium positions of the particles. [20]. Moreover, lateral forces perpendicular to the flow direction are crucial for manipulating particles [8]. Researchers have explored spiral microchannels to minimize the number of focusing lines for more efficient particle separation [21, 22]. However, designing spiral microchannels poses challenges due to unpredictable forces like inertial lift and Dean drag forces, which vary with channel dimensions, particle size, and flow rate [22]. Current design methods rely heavily on experiments, leading to costly iterations. Thus, overcoming these challenges is essential for improving separation efficiency and purity. Therefore, the present study aims to evaluate the effectiveness of adjusting Dean flow intensity and direction in spiral microchannels based on previous research findings. This review seeks to assess how well this strategy works by looking at what earlier researchers have done and discovered.

Several review papers have been published about the manipulation of fluid flow and particle movement in microchannels, focusing on inertial microfluidics, discussing topics such as Dean flow and particle or cell separation mechanisms, reflecting the ongoing research interest in this area. In 2019, Chung [23] conducted a mini-review discussing the physics of inertial microfluidic systems, with a specific emphasis on inertial particle migration and secondary flow. In 2020, Zhao et al. [8] extensively explored the phenomenon, theory, and applications of secondary flow in inertial microfluidics. Their review article delved into the utilization of Dean flow a type of secondary flow generated by various designs such as microchannels with obstructions, spirals, serpentines, and double-layered channels with a groove array. In a review article, Nasiri et al. [15] in 2021 outlined the principles and uses of commonly employed label-free microfluidic-based cell separation techniques. The article summarized the various applications of microfluidic methods for separating circulating tumor cells, blood cells, immune cells, stem cells, and other biological cells. It also delved into computational approaches that complement these microfluidic methods. In 2023, Saffar et al. [24] conducted a review study on the physics of Dean vortices, examining the factors that affect the number and arrangement of these vortices. They investigated how geometrical parameters, such as cross-section shape, aspect ratio, and radius of curvature, influence the Dean vortices. Additionally, they gathered various methods for calculating the Dean number in order to mitigate potential misinterpretations arising from the lack of a standardized formula for this dimensionless number, reflecting the effects of inertial and centrifugal forces in comparison to viscous forces on fluid flow. Previous studies have investigated the fundamental mechanisms behind the formation of Dean vortices in various microchannel geometries, examining how key parameters like geometric and operational factors influence the intensity, position, and number of these vortices. However, none of these studies have explored the effects of vortex intensity and position on the final equilibrium position of particles across the microchannel cross-section. This means that there is a gap on the examination of the effect of the Dean vortices intensity and shape on the particle movement within the spiral microchannels. This knowledge gap is crucial for researchers seeking to optimize microchannel design for more effective particle separation and manipulation. The present review article's concept could fill this important gap in existing literature. It is worth noting that the focus here is mainly on spiral microchannels and specifically explores the impact of geometrical parameters on the particles' equilibrium position. It will be discussed how controlling the intensity and direction of Dean flow in spiral microchannels plays a pivotal role in shaping particle behavior and filtration outcomes. This means that through adjusting Dean flow parameters, such as shape and intensity, researchers can potentially predict

particle trajectories and equilibrium positions without solely relying on extensive experimental or numerical studies. By understanding the relationship between Dean flow and particle behavior, researchers can optimize microchannel designs for efficient particle filtration, paving the way for predictive modeling and improved filtration performance.

Notably, there is currently a scarcity of comprehensive technical reviews on the techniques employed by researchers to exert greater control over the trajectory of particles within these microchannels. This article presents a comprehensive exploration of the principles of filtration and the mechanics behind inertial microfluidic techniques utilized in spiral microchannels. It delves into the complexities of channel aspect ratio (AR), particle size, cross-sectional geometry, and the influence of channel loop patterns on particle equilibrium within spiral microchannels. Considering the secondary flow mechanisms in different structured channels with spiral geometry, particle manipulation is discussed in detail. The spiral microchannel structures can be classified based on their cross-section shapes and loop patterns, each representing distinct mechanisms of particle manipulation within the channels. This classification is depicted in Fig. 1, elucidating the fundamental methodologies for designing spiral microchannels. The review culminates by delineating the essential findings and outlining the future research directions in this field.

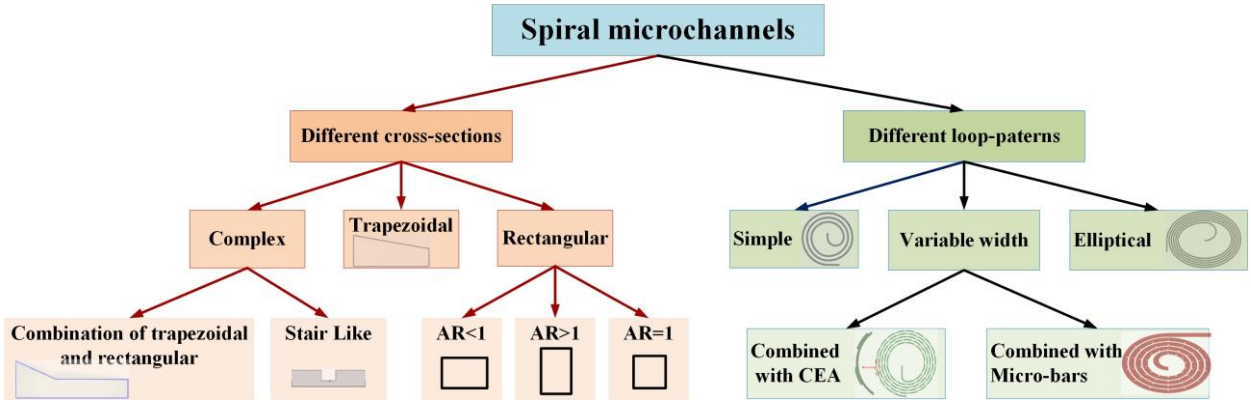

Fig 1: An illustration depicting the categorization of spiral microchannels. The figure shows the division of spiral microchannels into two categories based on their cross-section shape and loop pattern. Within the classification of the spiral microchannel cross-section, the aspect ratio (AR) represents the ratio of the height to width.

2. Mechanisms of Filtration

In microfluidics, inertia and viscosity play key roles beyond the traditional Stokes flow assumption. The middle regime, between Stokes and inviscid flow, brings forth unique inertial effects including inertial migration of particles and secondary flows in curved channels [19]. These effects play vital roles in inertial microfluidics technique and are discussed in the following sub-sections.

2.1. Inertial migration of particles

In confined channel flows, manipulation of cells and particles through inertial forces is possible, influenced by various factors such as channel dimensions, aspect ratio, particle diameter, and flow rate [19, 25]. In straight microchannels, particle migration is driven by inertial lift force (F_L) proportional to $\rho U^2 a_p^4 / H^2$, where ρ , U , a_p , and H represent fluid density, velocity, particle size, and channel height, respectively [20]. Liu et al. [26] in 2015 studied the inertial migration and focusing of 15 μm spherical particles in rectangular microchannels at various Reynolds numbers (Re), showing different focusing behaviors based on channel aspect ratios (AR), and flow rates, which are shown in Fig. 2a. As shown in this figure, in square microchannels ($AR = 1$), particles focus near walls at four equilibrium positions. In high AR microchannels ($AR \geq 2$), 15 μm particles focus at long wall centers at low Re and shift towards the side wall at high Re . Higher AR straight microchannels reduce the number of focusing lines compared to square microchannels, but the number of stable equilibrium positions increases past a critical Reynolds number due to changes in inertial lift force coefficient on the particles. The critical Reynolds number (Re_c) was found as $\mathrm{Re}_c = 697(AR/k)^{-0.79}$, where k denotes the ratio of particle size to channel height [26]. The reason for this can be explained by looking at how the lift force coefficient changes at different Reynolds numbers. For a channel with an AR of 4, the changes in the inertial lift force along the long wall (z -direction) can be explained. The lift force is a monotonically decreasing function of z and is negative along the entire axis at $\mathrm{Re} = 50$, leading to focusing at the centers of the long walls as depicted in Fig. 2b. The lift force

profile undergoes a significant change with increasing Reynolds number. At Re values between 100 and 300, the lift forces increase significantly in magnitude between the center and the wall, forming a second negative slope on the lift curve. This leads to a stable equilibrium position between the positive peak and the wall. The high Re flow's inertia causes the sign reversal of the lift force, with the inviscid effect becoming more pronounced near the wall as Re increases. Acceleration of the fluid between the particle and the wall results in a Bernoulli-like effect, creating low pressure on the wall side of the particle. In the lateral migration of particles, pressure force dominates over viscous force [26].

When particles flow through curved channels, they undergo inertial migration influenced by secondary Dean flow. Dean flow in curved microchannels manifests as swirling motion due to varying fluid velocities across the channel's cross-section. This swirling motion, resembling symmetrical whirlpools, is fundamental to understanding Dean flow phenomena in curved microchannels [19, 27]. In a curved channel, secondary flow occurs due to velocity differences between center and near-wall fluid. Fluid near the center moves faster, creating outward inertia and a radial pressure gradient. Stagnant fluid near walls cycles inward due to centrifugal force, forming symmetric vortices [19].

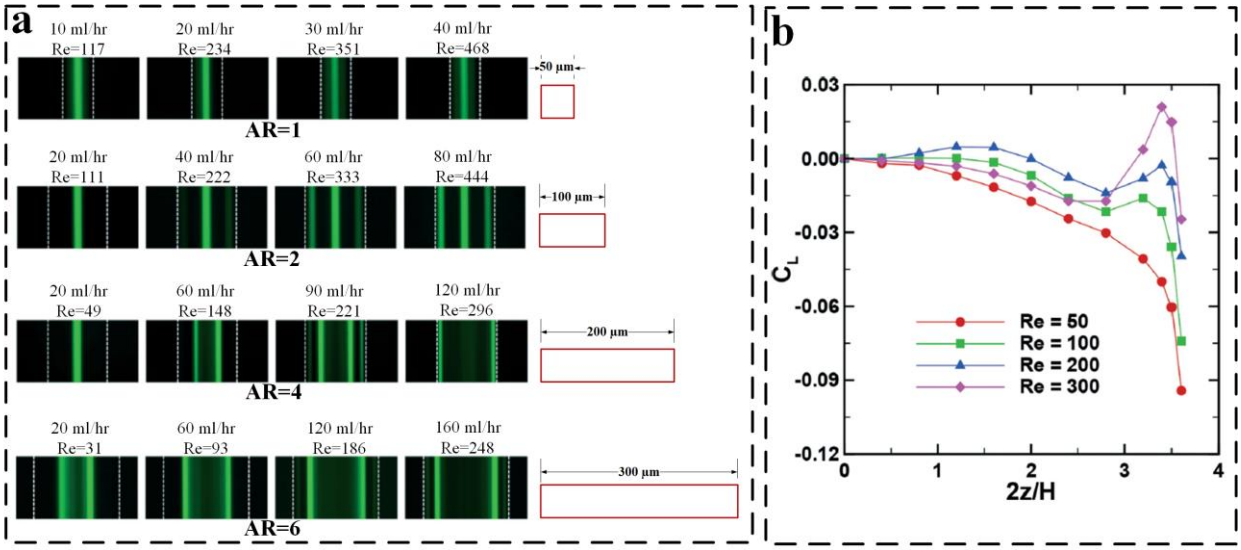

Fig 2. a) Fluorescence picture displaying the stable locations for 15 μm particles, shown in green lines, with various aspect ratios (AR), Reynolds numbers (Re), and flow rates presented in the study conducted by Liu et al. [26]. b) The lift force coefficient profile for 15 μm particles in a channel with AR of 4 at various Re [26].

Vortices in the Dean flow induce lateral particle transport along the width-direction of the channel cross-section, thereby influencing the equilibrium position of particles. The imparted force varies with particle size similar to inertial lift phenomena. Moreover, secondary flows have been observed in diverse microchannel geometries, such as straight microchannels with contraction-expansion arrays, serpentine microchannels, and spiral microchannels [28]. The magnitude of this flow can be quantified using a dimensionless number introduced by Dean [28] given by [21]:

$$De = \frac{\rho U_F D_H}{\mu}\sqrt{\frac{D_H}{2R_c}} = \mathrm{Re}\sqrt{\frac{D_H}{2R_c}}, \quad (1)$$

where, ρ, U_F, μ, R_c, and D_H stands for the fluid density, average flow velocity magnitude, fluid viscosity, radius of curvature of the channel path, and channel hydraulic diameter, respectively. Additionally, Re is the Reynolds number of the flow. A particle in curved channels experiences combined effects of inertial migration and secondary flow. The drag force depends on the local secondary flow velocity field (U_D) which is perpendicular to the primary flow. The lateral migration velocity magnitide of the particles in a spiral microchannel relies on the Dean number, and its computation can be determined as follows [21]:

$$U_D = 1.8\times10^{-4} De^{1.63} \quad (2)$$

The competition of Dean drag force with net of lift forces determines the equilibrium position of particles. The ratio of these forces (R_f =inertial lift force/Dean drag force) describing behaviour of particle movement in these systems, by considering the following cases [19]:

1. R_f approaches 0; in this case, particles are entrapped into the secondary flow and not focused within the spiral microchannel. The red blood cells swirling with the Dean cycles in the study conducted by Warkiani et al. [21] is an example of this case. In fact, the particles or cells are small enough that their movement is affected by the Dean drag force and not affected by the lift force.
2. If R_f approaches infinity; for sufficiently high particle Reynolds numbers, particles migrate to inertial focusing equilibrium positions independent of the secondary flow. The focusing of particles in straight microchannels refers to this extreme case.
3. Intermediate R_f , Leads to new focusing modes and applications, like circulating tumour cells in spiral microchannels of Warkiani et al. [21].

More information about these three cases is provided in section 3-1.

2.2. Force calculation

Understanding and controlling particles in spiral microchannels involves predicting forces that influence their behaviour under fluid flow. Inertial migration is well-known for the interaction of two inertial effects including: 1) the shear gradient lift force, which pushes particles away from the center of the channel due to the fluid's speed profile curvature, and 2) the wall lift force, which pushes particles away from the channel walls due to their interaction with the flow [20, 29]. Due to wall effects, there is a delay between the particle and the flow. The curvature causes a significant difference in relative velocities between the wall side and the opposite side of the particle, based on the parabolic fluid velocity profile. This difference creates a shear gradient lift force due to lower pressure on the wall side, pushing particles towards the wall. Eventually, a balance is reached with the wall-induced lift force, leading to an equilibrium position. The parabolic velocity profile of fluid flow causes two extra lift forces: Magnus lift force and Saffman lift force [8]. The following sub-sections cover the calculation method for the Dean drag force and the efforts to calculate the lift force on particles.

2.2.1. Viscous drag force

Selecting the right drag law requires confirming its validity based on the relative Reynolds number of particles in the flow, denoted as Re_r . It can be calculated using Equation 3 [30, 31], where a_p is the particle diameter, u is the fluid velocity at the particle's position, and v is the particle velocity.

$$\mathrm{Re}_r = \frac{\rho |u - v| a_p}{\mu}, \tag{3}$$

Strictly speaking, u represents the velocity of the fluid at the particle's position in the absence of the particle, unless interactions between the fluid and particle are considered. In situations with very low particle Reynolds number in creeping flow ($\mathrm{Re}_r \leq 1$), the Stokes drag law applies. Consequently, drag forces (F_D) on particles can be estimated using the Stokes drag law depicted in Equation 4 [30, 31].

$$F_D = 3\pi\mu a_p (u - v) \tag{4}$$

2.2.2. Lift force

Initially, studies on asymptotic solutions were centerd on addressing the migration of spherical particles in planar fluid flow (Ho & Leal, 1976 [32]; Saffman, 1965 [33]; Tam & Hyman, 1973 [34]). Back in 1976, Ho and Leal [32] were the pioneers in suggesting a specific formula for the inertial lift force acting on particles in a 2D plane Poiseuille flow. In their work, they introduced a formula ($F_L = C_L \rho U_m^2 a_p^4 / H^2$) in which the symbols C_L , ρ , a_p , and U_m denote the lift force coefficient, fluid density, particle size, and maximum fluid velocity, respectively. However, this formula's limitation ($a_p / H \ll 1$) lies in its applicability to microfluidics due to the restriction where particle size is often similar to the channel size, making direct application challenging [32]. However, with the increasing diversity and complexity of microfluidic applications in particle sorting and focusing, it has become crucial to investigate the real particle migration in confined microchannel flow. As a result, a novel asymptotic equation was proposed to study the lateral migration of buoyant particles in 2D confined flow across a wide range of Reynolds numbers (Asmolov, 1999 [35]). In 2009, Di Carlo et al. [36] conducted a thorough quantitative analysis of inertial lift in a square channel. Their findings indicated that the inertial lift force can be expressed as $F_L = C_L U_m^2 a_p^3 / H$ in the vicinity of the channel center (when $x/h < 0.5$, where x is the distance of the particle position to the channel center in the width direction of the cross-section of the channel, and h is the half of the

channel width), and $F_L = C_L \rho U_m^2 a_p^6 / H^4$ nearing the channel wall. Notably, they verified the validity of this scaling law for $a_p / H > 0.1$ [36]. Moreover, in 2015, Hood et al. [37] introduced an influential asymptotic model to predict how particle size affects the focusing position. This versatile model is suitable for a broad spectrum of particle sizes and Reynolds numbers. They suggested incorporating a correction term of $O(a^5)$ to expand on the scaling law proposed by Ho and Leal [32] for particles of finite size. The asymptotic approach allows for the computation of focusing forces acting on particles positioned at arbitrary locations within the three-dimensional (3D) channel, achieved through the development of a perturbation series expansion for the lift force. The asymptotic model expressing the lift force and presented by Hood et al. is obtained as [37]:

$$F_L = \rho U_m^2 c_4 a_p^4 / l^2 + \rho U_m^2 c_5 a_p^5 / l^3 \tag{5}$$

where a 3D Poiseuille flow with density of ρ was modeled in a long square channel with a width of l. The unaltered center-line velocity of the flow when unaffected by a particle (with a size of a_p) is represented by U_m. In equation (5), c_4 and c_5 are constants which are calculated based on the fluid flow field [37]. Su et al., [25] (2021) introduced a rapid numerical algorithm integrating machine learning for inertial microfluidic device analysis and design. They utilized direct numerical simulation (DNS) to build an inertial lift force database in diverse microchannel conditions. Their machine learning model forecasts inertial lift distribution based on channel geometry, Reynolds number, and particle blockage ratio. The study by Su et al. [25] has limitations in parameter scope for the lift force coefficient, valid in $1 \le AR \le 4$, $0.1 \le k \le 0.3$, and $50 \le \mathrm{Re}_{Su} \le 200$ constraints, where AR is aspect ratio, k is particle blockage ratio, and Re_{Su} is Reynolds number defined in the study of Su et al. [25] ($\rho U_{\max} H / \mu$, where $U_{\max}$ is the maximum fluid velocity in the channel) [25]. In 2023, Su et al. [38] explored the impact of Reynolds number and particle blockage ratio on inertial lift force coefficient. They introduced a decomposition of inertial lift force (F_L) into pressure-induced lift force (F_{LP}) and viscosity-induced lift force (F_{LV}), with $F_L = F_{LP} + F_{LV}$. By integrating pressure and viscous stresses on the particle surface, they derived a formula for the inertial lift coefficient $C_L = F_L / (\rho U_m^2 a_p^4 / H^2)$ which is as [38]:

$$C_L = \left(2.6\,\mathrm{Re}^{-0.32} + \mathrm{Re}^{-0.55}(a_p/H)^{-1}\right)(y/H) - \left(\frac{2.6}{1+e^{-\alpha(\frac{y}{H}-\beta)}} - \gamma\right)(a_p/H)^{n_w} \tag{6}$$

Here, y represents the particle distance to the channel center, while α, β, γ, and n_w depend on the Reynolds number and particle position in a square microchannel cross-section. This formula is valid for flow Reynolds numbers up to 400 and particle blockage ratios up to 0.25, with applicability extending to rectangular cross-section microchannels.

In summary, researchers have made strides in numerically exploring inertial migration of particles, from studying asymptotic solutions to developing novel equations and numerical algorithms, which aid in understanding and designing inertial microfluidic devices. However, each of the presented methods is applicable for a certain condition regards to the ranges of Reynolds number, particle size, and aspect ratio of the spiral microchannels.

2.3. Examination of the fluid flow field

To determine the lift forces and Dean drag force acting on particles due to fluid flow within spiral microchannels, it is essential to first calculate the fluid flow field. The particle tracing through the microchannels involves employing Navier-Stokes-based solutions. The calculation of the fluid flow field within the microchannels requires solving the Navier-Stokes equations and the Continuity equation. Commercial computational fluid dynamics (CFD) packages can be utilized for both the calculation of the fluid flow field and the tracing of particles using Newton's second law [39]. For instance, Hou et al. [40] in 2013, investigated the isolation of circulating tumor cells from whole blood both numerically and experimentally in a study conducted. In their numerical analysis, they utilized the commercially available COMSOL Multiphysics software to solve the fluid flow and track the particles. The results of the particle tracking were subsequently validated against experimental data.

Moreover, it can be considered exploring the use of advanced computational fluid dynamics (CFD) simulations combined with machine learning algorithms to optimize the shape, location, and strength of Dean vortices in complex spiral microchannels with different shapes of cross-sections or loops patterns. In the following sub-section, the use of artificial intelligent in different field of study, especially microfluidics, is explained.

2.3.1. Use of artificial intelligence (AI) algorithms in microchannel design

Machine learning involves teaching computers to learn from existing data, often using artificial neural networks to develop highly accurate predictive models. This technology has seen widespread application across various fields. Today, artificial intelligence (AI) and deep learning (DL) are commonly utilized in many areas of study. These include the analysis of structural mechanics problems (Gaur et al., [41] in 2022), solving continuous time-varying matrix inversions (Shi et al., [42] 2023), identifying liquid-liquid flow patterns in microchannels (Shen et al., [43] 2020), the potential and application of deep learning in image analysis (Gheisari et al., [44] 2023), data-intensive modeling to reduce memory requirements and computation time (Luo, [45] 2024), as well as the development of a computational framework for designing complex nano-composites (Liu and Lu, [46] 2022).

Some researchers used machine learning to trace or sort particles or cells within the microchannels. For example, in the study conducted by Raymond et al. [47] in 2020, researchers explored the use of acoustic waves for precise positioning of cells and particles due to their biocompatibility and ability to induce microscale force gradients. While traditional acoustic fields are limited to periodic grids, a recent development showed that interaction between microfluidic channel walls and surface acoustic waves can create spatially varying acoustic fields, allowing control over pressure fields. To address the challenge of designing channels for specific acoustic patterns, the researchers employed a deep learning technique using a deep neural network (DNN) to quickly generate desired acoustic patterns through microchannel elements. This DNN was trained on images of pre-solved acoustic fields. Subsequently, they utilized the trained DNN to design innovative microchannel structures for precise microparticle arrangement [47]. Su et al. [25] in 2021 developed a numerical algorithm that utilizes machine learning techniques to analyze and design inertial microfluidic devices. They first generated a database of inertial lift forces by conducting DNS in straight microchannels with rectangular, triangular, and semicircular cross-sectional shapes over a wide range of operating parameters. Then, they used artificial neural network (ANN) modeling to train complex fitting model and extrapolation based on the obtained database. Finally, the machine learning model was used to predict the distribution of the inertial lift force in channel cross-section for any given conditions within the considered parameter space [25]. Fig. 3 provides an overview of the prediction process steps.

Based on the reviewed articles mentioned earlier, it is evident that artificial intelligence and deep learning can be employed for channel design and predicting particle trajectories through microchannels. For instance, the method presented by Gaur et al. [41] in 2022 can be utilized to examine the channel structure and stress on the channel walls. To calculate the inertial lift force acting on particles and trace their paths, the study by Su et al. [25] in 2021 is a notable reference. Additionally, methods explored by Lou [45] in 2024 can be used to reduce the memory and time required to solve the equations for calculation of fluid flow field and simulating the particle trajectory within the microchannels.

3. Particle or cell filtration using conventional spiral microchannel

Di Carlo [19] discussed fluid dynamics and inertial migration in curved microchannels in 2009. The importance of transversal flows in microchannels for precise fluid flow control to improve mixing or separation goals was emphasized in the study. Kuntaegowdanahalli et al. [11] also in 2009 studied an inertial microfluidic device using Dean-coupled inertial migration in spiral microchannels for continuous multi-sized particle separation. The device combined inertial forces with Dean rotational force, leading particles to a single equilibrium position near the inner microchannel wall based on the inertial lift to Dean drag forces ratio. This study presented the first spiral lab-on-a-chip (LOC) for size-dependent separation [11]. Various research has analyzed particle behavior in spiral microchannels, exploring how factors like particle size, channel aspect ratio, and spiral microchannel design affect particle positioning and Dean flow. The subsequent discussion examines the specific impacts of these parameters. At the end of the sub-sections, Table 1 shows the summary of all discussions.

3.1. Effect of particle size on the equilibrium position of particles

Studies have explored how particle size affects its equilibrium position. When particles are smaller than 0.07 times the microchannel height, they get trapped in Dean flow and aren't focused effectively. This finding was observed in studies on separating small from large particles (Bhagat et al., [48] in 2008) and isolating circulating tumour cells (CTCs) from blood cells (Warkiani et al., [21] in 2016). The results of both studies are presented in Fig. 4a and 4b, respectively. In the study conducted by Bhagat et al. [48], a 5-loop spiral microchannel effectively separated 1.9 μm and 7.32 μm particles which introduced to the channel form inner inlet as shown in picture I of Fig. 4a. As shown in picture II of Fig. 4a, Larger particles (Green line) focused in a line near the inner wall due to inertial lift force over Dean vortices, while smaller particles (Purple line) collected at the outer outlet. The distribution of 1.9 μm particles at the outlet lacked strong focusing. The interaction between inertial lift force and Dean drag force in their proposed spiral microchannel is shown schematically in picture III of Fig. 4a [48]. In

Warkiani's study [21], a spiral microchannel isolated circulating tumour cells (CTCs) from blood cells illustrated schematically in picture Ⅰ of Fig. 4b. CTCs were found to focus in a line near the inner outlet, depicted in picture Ⅱ of Fig. 4b, while blood cells exhibited migration through Dean vortices and ultimately exited through the outer outlet in a broad band as illustrated in picture Ⅲ of Fig. 4b. [21]. Both studies [21, 48] used a similar design method to maximize the distance between large particles (or target particles) and small particles (which are not focused) by adjusting the channel length. This method is explained in section 4.

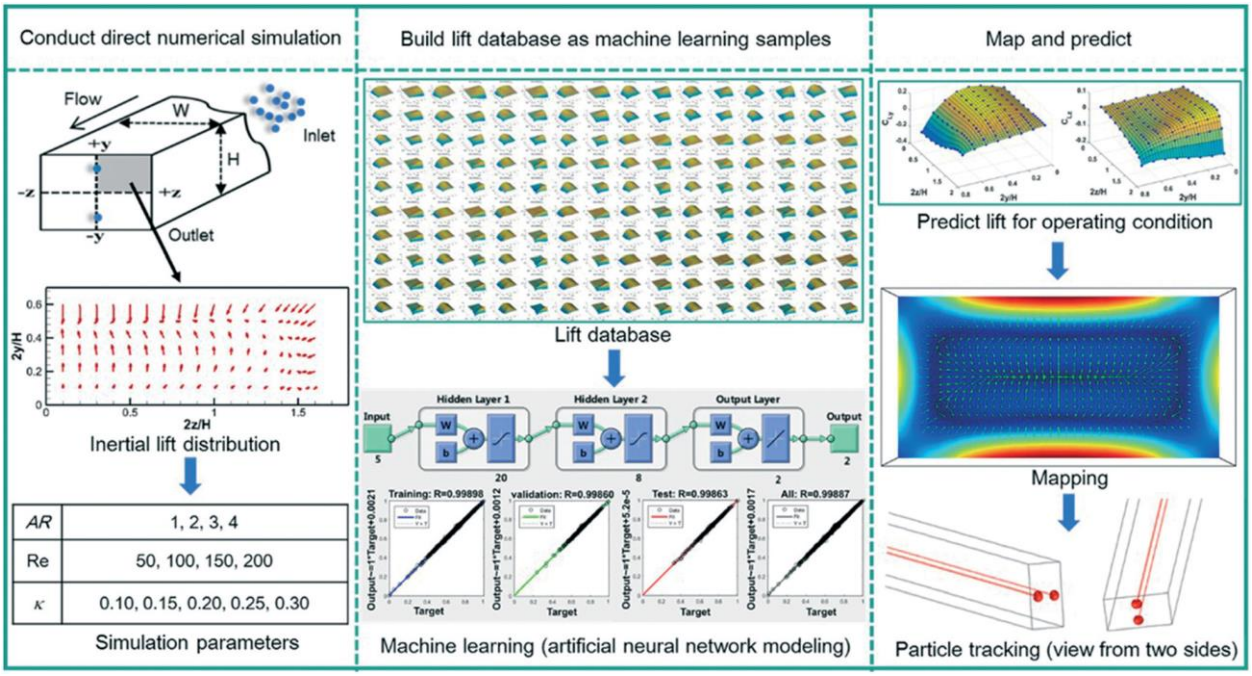

Fig 3. A three-step overview of the prediction process proposed by Su et al. [25] is illustrated in three columns. Step 1: Direct numerical simulations were used to calculate the distributions of inertial lift forces on spherical particles in the cross-sections of rectangular microchannels, across a wide parameter space as shown in the table. Step 2: The simulation results were compiled into a force database, which was then used as training data for a machine learning model. Step 3: The trained prediction model was used to determine the distribution of inertial lift forces, which were then mapped onto the cross-section to predict particle trajectories.

Employing an alternative technique to separate microparticles by size ensures precise focusing of particles of various sizes, offering a distinct method for particle separation. Yoon et al. [49] in 2009 found that at normalized heights of 0.27 and 0.72, zero velocities consistently occur, leading to size-selective separation as shown in Fig. 4c. In this regard, the large particles experience a force from the outward velocity through the lateral flow, while the smaller ones are dominantly forced by inward velocity as depicted in Fig. 4c. This leads to big particles moving towards the outer wall and the smaller particles moving towards the inner wall as they travel through the curved rectangular microchannel. This different movement of the particles results in the continuous separation of particles based on their size using secondary flow. In their study, the trajectory of 20- and 40-micrometer particles was examined in a curved channel with a height and width of 75 μm and 150 μm , respectively, showing that smaller particles, less than 0.27 of the channel height, tend to focus near the inner wall of the curved channel [49]. It should be mentioned that in the study by Yoon [49], all particles, including small and large ones, pass the criteria of ($a_p/H > 0.07$) against the studies of [21, 48]. The research of Guzniczak et al. [50] also confirmed the importance of the zero velocities mentioned by Yoon et al. [49] in the final equilibrium positions of the focusable particles. Guzniczak et al. [50] found in 2020 that larger cells with a confinement ratio of $a_p/H > 0.26$ move toward outlets near the outer wall in spiral microchannels.

Overall, the studies revealed that not all particles can be successfully focused through conventional spiral microchannels. Only particles larger than 0.07 times the microchannel height can be effectively focused. Additionally, it can be concluded from the researches that the equilibrium position of these focusable particles significantly depends on their size. The studies showed that particles larger than 0.27 times the channel height are influenced by the direction of the transversal fluid velocity, leading to their focusing line being closer to the outer

channel wall.

3.2. Effect of Aspect ratio on the equilibrium position of particles

The width and height of a spiral microchannel crucially impact particle equilibrium position for separation. The height-to-width ratio, or aspect ratio, is a crucial factor analysed by Kuntaegowdanahalli et al. [11] in 2009. They studied particle separation in a low aspect ratio Archimedean spiral microchannel to understand the interaction between Dean drag force and inertial lift force on particle positioning. As shown in Fig. 5a, by changing the channel height (90-140 μm) while maintaining a constant width of 500 μm , they found that the particle stream moved away from the channel wall with increasing Dean number (De), showing Dean force dominance. Higher flow velocity (U_f) increased the lift force ($F_L \propto U_f^2$) relative to Dean drag force ($F_L \propto U_f^{1.63}$), but a decrease in lift force coefficient at higher velocities reduced the net lift force, shifting the stream from the wall. Therefore, as shown in Fig. 5a, higher flow velocity which results increasing Dean number gets the particles closer to the channel center. It's noteworthy that the lift force coefficient is typically below one, decreasing with rising flow velocity or Reynolds number. Raising the channel height concentrated particles away from the inner wall due to increased Dean drag force and reduced lift force. Hence, modifying the Dean number or channel height at a specific velocity can alter particle stream position [11].

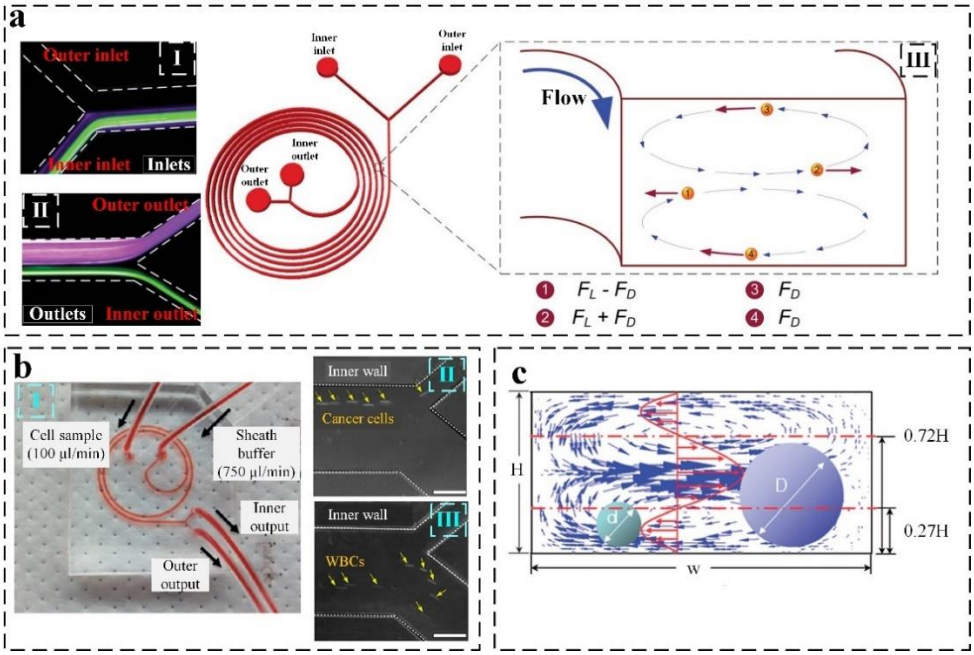

Fig 4. Effect of particle size on particle equilibrium position: (a) This figure illustrates the spiral microchannel utilized by Bhagat et al. [48], showing the positions of fluorescent-labelled polystyrene particles (1.9 μm and 7.32 μm) at the inlets (I) and outlets (II) within the channel. It also highlights the presence of Dean vortices and the interplay between the inertial lift force and Dean drag force. b) Image I shows the complete spiral device used by Warkiani et al. [21]. Images II and III exhibit the final focusing position of CTCs and the eventual location of WBCs at the outlet, respectively. c) Study by Yoon et al. [49] demonstrates size-based micro particle separation using fluidic forces in the channel's cross-sectional velocity distribution.

In 2012, Martel and Toner [51] studied the impact of the aspect ratio of low aspect ratio spiral microchannels by adjusting the width of the channel (the ratio of width to height of channel ~ 1 to 8). They analysed how particles behaved in curved microchannels, considering the inertial lift force and Dean drag force. As shown in Fig. 5b They found that wider spiral microchannels have a more flattened flow field, lower shear gradient, at constant fluid velocity. Moreover, wider channels experience a stronger Dean drag force on particles, causing the particles to be focused closer to the inner wall [51]. Fig. 5b shows the effect of wider channel cross-section on the lateral velocity creates by Dean flow. In advancing the studies, the researchers endeavoured to devise a method for regulating or predicting the intensity of the inertial lift and the Dean drag forces within conventional spiral microchannels. In this regard, the effect of fluid velocity on the forming of Dean vortices was examined by some researchers. In a 2017 study by Nivedita et al. [52], investigated Dean flow vortices in low-aspect ratio spiral microchannels, focusing on

their behaviour relative to the channel aspect ratio and Dean number. The study revealed the presence of secondary Dean vortices beyond a critical Dean number (De_c), highlighting the impact of fluid flow rate on Dean vortex development. They observed that under a critical Dean number, only two counter-rotating Dean vortices were formed, while more than two vortices appeared beyond this critical value. The research findings indicated that the De_c is highly influenced by the AR ($De_c \propto AR^{-0.5}$). In Fig. 5c, the effects of Dean number and channel aspect ratio on formation of secondary Dean vortices are illustrated using a diagram. Additionally, the study looked at how high Dean numbers affect the position of red blood cells in a microchannel. It found that as the flow rate increases, secondary Dean flows move the RBCs from the inner wall to the outer wall of the channel [52]. In a separate work by Cruz and Hjort [53] in 2021, they demonstrated that inertial focusing can be achieved in high aspect ratio curved Systems (HARC systems). This technique not only concentrates randomly distributed particles into a single position but also enables size-based separation with theoretically infinite resolution, experimentally proven up to 80 nm . The experimental results aligned well with the proposed model, allowing for precise system engineering. While HARC systems can effectively focus particles with moderate changes in system parameters, achieving particle separation necessitates careful design, precise fabrication, and stable operation. Although the research group achieved high separation sensitivity, their system showed limitations in separating particles smaller than 1 μm , potentially restricting its applicability to a certain particle size range [53].

Overall, in low aspect ratio spiral microchannels, increasing the channel's height or decreasing its width brings the line of focused particles closer to the center of the channel, when the average fluid velocity remains constant. The flow rate of the fluid greatly influences the interplay between Dean drag and inertial lift forces, consequently determining the final position of particles. Augmenting the fluid flow rate moves the particles closer to the centerline of the spiral microchannel. Researchers have introduced the dimensionless number De_c , which determines the occurrence of secondary Dean vortices. These vortices influence the position of the particle focusing lines.

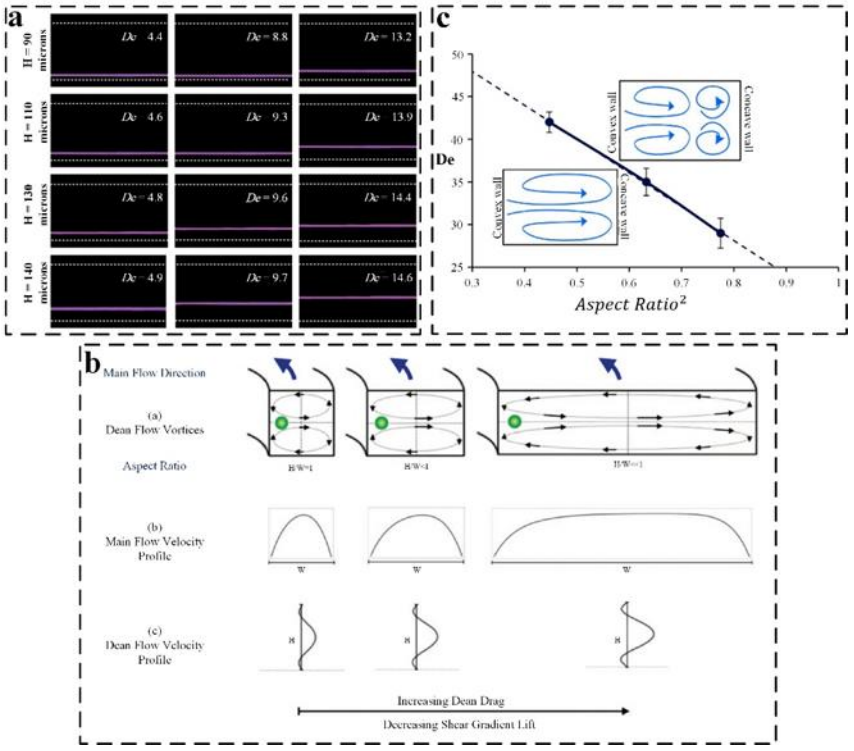

Fig 5. Effect of the aspect ratio of the low-aspect ratio spiral microchannel on the equilibrium position of the particles. a) Fluorescent images illustrating the position of the focused 10-micron particle stream in spiral microchannels of different heights at varying Dean numbers presented by Kuntaegowdanahalli et al. [11]. b) Illustration showing various flow patterns in curved channels of varying widths under inertial focusing velocities as detailed in the study by Martel and Toner [51]. c) Graph showing how the critical Dean number changes with the aspect ratio of a rectangular channel [52].

3.3. Effect of cross-sectional shape on Dean flow

Rectangular cross-sections: In the field of microfluidics, spiral microchannels with rectangular cross-sections have gained popularity due to their effectiveness in separating cells or particles and ease of fabrication. Researchers have observed that the stability of Dean vortices in these channels decreases as the curvature radius increases along the channel. This issue leads to less effective manipulation and control of particle trajectories, potentially impacting the efficiency of size-based separation processes. To overcome this limitation, researchers are exploring methods to modify the shape and intensity of Dean vortices. One approach involves investigating the impact of cross-sectional shape variations in spiral microchannels.

Trapezoidal cross-section: Scientists are more interested in trapezoidal cross-sections due to their ability to improve separation sensitivity. This sensitivity refers to how effectively particles are separated with these cross-sections and denotes the space between the focusing lines of particles created using these cross-sections [54]. In 2018, Al-Halhouli et al. [55] created a spiral microchannel with a trapezoidal cross-section. This design encouraged Dean vortices, boosting separation efficiency. A comparison between separating particles of different sizes using rectangular and trapezoidal cross-section spiral microchannels is illustrated in Fig. 6a. As shown in this figure, the cores of Dean vortices in the trapezoidal cross-section shifted towards the outer wall and impacts the equilibrium position of particles based on their size; consequently, leads to higher separation sensitivity than a rectangular cross-section. The movement of smaller particles toward the outer wall and the stabilization of larger particles closer to the inner wall were observed as a consequence of the intricate interplay between Dean drag and lift forces. For small particles, the Dean drag force predominated, while for larger particles, the lift force was more significant, thereby boosting separation efficiency. The equilibrium positions of particles with sizes of 5, 10, and 15 μm were analyzed. The results revealed that 5-micron particles were primarily concentrated near the outer wall, whereas the 10 and 15-micron particles tended to be closer to the inner wall, particularly at flow rates exceeding 1 $ml/\min$. The trapezoidal cross-section improved separation sensitivity compared to a rectangular cross-section but allowed only binary separation. Notably, no separation was observed between 10- and 15- μm particles at flow rates ranging from 1 to 5 $ml/\min$. The fabrication of the chip to achieve the desired results is crucial, as the chip must operate at high pressure. To this end, the researchers fabricated the chip using femtosecond laser ablation in glass. Nevertheless, the accessibility to such a laser system poses a challenge [55].

Complex cross-section: In some studies, the researchers considered a complex cross-sectional shape for their spiral microchannels. In a study led by Ghadami et al. [56] in 2017, a spiral microchannel with a stair-like cross-section was proposed to improve both particle separation resolution and throughput, compared to a traditional spiral microchannel with a rectangular cross-section. The schematic of the innovative microchannel featuring a stair-like cross-section, developed by this research group [56], is illustrated in picture I of Fig. 6b. This enhancement was accomplished by carefully managing the shape and placement of Dean vortices. The streamline within the spiral microchannel featuring a stair-like cross-section is illustrated in image II of Fig. 6b. In this configuration, the two vortices are distinctly arranged along the longitudinal direction. The distribution of vortices in the proposed spiral microchannel differed from that in a standard spiral microchannel, as shown in Fig. 6b. The researchers examined the separation of 7.32 μm and 20 μm particles using their proposed microchannel. They observed that at flow rates between 2000- and 2304 $\mu l/\min$, small and large particles reached different equilibration points within the channel. At flow rates below 2000 $\mu l/\min$, particles were trapped near the inner wall vortex, while for flow rates above 2304 $\mu l/\min$, particles migrated towards the outer vortex, passing through the intermediate channel section. The team achieved a 260 μm gap between the equilibrium positions of the two particle sizes at a flow rate of 2304 $\mu l/\min$.To study how vortices impact particle separation in stair-like cross-sections, a higher fluid flow rate is needed. This is because the flow rate affects how the fluid flows sideways. When the flow rate goes up, the dead zones on both sides get bigger [57], shrinking the Dean vortices. Consequently, more fluid flows from the inner to the outer wall, boosting the chances of particles migration at higher flow rates. Additionally, due to the cross-section's shape and the presence of the middle part, vortices form in a series along the channel. This traps small and large particles in separate vortices, improving the separation sensitivity. In contrast, a study by Nivedita and Papautsky [58] in 2013 demonstrated that a conventional spiral microchannel, with the same dimensions, could separate 7.32 μm and 20 μm particles at a flow rate of 1800 $\mu l/\min$, with a separation distance of 95.6 μm. Thus, Ghadami et al. [56] proved that the stair-like cross-section spiral microchannel significantly improves both separation efficiency and throughput compared to the conventional design. However, this enhanced separation occurs within a specific flow rate range and is not as gradual or effective at lower flow rates.

In 2020, Mihandoust et al. [59] conducted a study on a spiral microchannel featuring a unique cross-sectional shape that integrated rectangular and trapezoidal sections. Their research aimed to efficiently concentrate particles

by addressing challenges associated with a confinement ratio greater than 0.07 ($a_p/H > 0.07$). The primary goal was to achieve precise particle focusing within a narrow band. The impact of various cross-section shapes on Dean vortices and particle equilibrium position is demonstrated in Fig. 6c. In the illustration, the trapezoidal section is positioned toward the inside of the channel and the rectangular section is located towards the outer part. The trapezoidal shape separates particles from the fluid, whereas the rectangular shape helps manage excess fluid and directs particle-free fluid towards the waste outlet. The Dean Vortex mechanism enhanced the focus in the trapezoidal region. The study introduced the concept of Complex Focusing Number (CFN) to quantify this effect, where higher CFN values indicate increased inertial effects in the channels. The experimental setup included spiral channels of 400-, 500-, and 600 μm widths, corresponding to CFN values of 4.3, 4.5, and 6, respectively. The findings demonstrated a 500-time increase in sample concentration in the 600 μm channel from the inlet concentration, with 98% separation efficiency (SE) [59]. However, the study did not explore separation applications using the proposed geometry. Moreover, they defined separation efficiency (SE) and complex focusing number (CFN) as [59]:

$$SE = \frac{\text{No. of particles collected in the target outlet}}{No.\text{ of particles collected from all outlets}} \tag{5}$$

$$CFN = \cot\alpha \frac{W_r}{W_t} \tag{6}$$

The selection of a spiral microchannel cross-section plays a crucial role in determining the equilibrium position of particles within the channel and influencing the formation of Dean vortices. Rectangular cross-sections offer simplicity in fabrication and analysis, leading to predictable particle equilibrium positions. However, their limited controllability over Dean vortices results in reduced efficiency in particle manipulation compared to other cross-sectional shapes. On the other hand, trapezoidal cross-sections enable efficient binary particle separation with high concentration and resolution. Yet, the fabrication challenges associated with trapezoidal shapes could potentially inflate production costs when compared to rectangular designs. Some researchers have investigated utilizing more intricate cross-sectional geometries to exert greater influence over the shape and intensity of Dean vortices for enhanced particle manipulation. These advanced cross-sections serve various purposes, such as facilitating high-throughput and high-resolution binary separations by forming secondary vortices or addressing challenges in focusing particles that do not meet the criterion of $a_p/H > 0.07$. However, the increasing complexity in fabricating spiral microchannels with intricate cross-sections poses a greater hurdle than with trapezoidal or rectangular designs. Furthermore, achieving precise control over the shape, position, and intensity of Dean vortices remains a subject of ongoing research and development in this field.

As evidenced by the prior works referenced in this section, improving the performance of spiral microchannels with advanced cross-sections requires optimization to achieve goals such as simultaneously achieving high throughput and high resolution in binary separation. To accomplish this, both geometric optimization and hydrodynamic control should be implemented. This entails optimizing the shape and dimensions of the cross-sections, alongside adjusting the flow conditions within the microchannels to enhance particle focusing and separation efficiency. Employing computational tools to simulate fluid dynamics, particle behavior, and separation processes can aid in refining the cross-sectional geometries. As detailed in sub-section 2.3.1, leveraging AI algorithms can be advantageous in cross-section design.

3.4. Effect of the spiral loops pattern on Dean flow

Another approach to address the issue of decreasing Dean flow intensity as the curvature radius of the spiral microchannel loop increases is to optimize the geometry of the spiral microchannels. Through geometric modifications, scientists strive to precisely regulate the intensity of Dean flow, leading to a more versatile microfluidic system. Shen et al. [60] in 2017 devised a sheathless microfluidic system with a spiral microchannel containing micro-bars to tackle issues with throughput, sheath fluid usage, and operational longevity. The top view of their device in picture I of Fig. 7a features a single-layer microchannel with a low aspect ratio that optimizes particle focusing through secondary flow acceleration. Results at a flow rate of 3 $ml/\min$ ($\mathrm{Re} = 200$) demonstrated successful concentration of particles of various sizes (7.3 μm, 9.9 μm, and 15.5 μm) into a single-stream near the inner channel wall. Increasing the flow rate to 5 $ml/\min$ resulted in particle migration, as smaller particles shifted closer to the outer wall. Picture II in Fig. 7a illustrates how flow rate affects particle positions. Particle positions correlate with the ratio of inertial lift force to Dean drag force ($F_L/F_D \propto a^3$). The technique achieved high throughput (up to 3 $ml/\min$) and stability (minimum 4 hours). However, existing inertial microfluidic channels

often face challenges with low throughput (<1 $ml/\min$) and limited operation time (<1 hour due to blockages and instability). Using their microchannel, particles exhibited high focusing efficiencies: 99.8% for 15.5-μm, 98.6% for 9.9-μm, and 90.9% for 7.3-μm particles at 3 $ml/\min$ ($\mathrm{Re}=200$). At 5 $ml/\min$ ($\mathrm{Re}=333.3$), particles migrated rapidly, leading to enhanced separation sensitivity. Higher flow rates like 6.5 $ml/\min$ ($\mathrm{Re}=433.3$) resulted in improved particle separation but risked splitting the stream into doubles due to high Reynolds number flow in the channel. The double or multiple stream lines for each particle size at $\mathrm{Re}=433.3$ is shown in picture II of Fig. 7a [60]. In a 2019 study by Gou et al. [61], they proposed a solution to overcome the challenge of reduction of the intensity of the Dean flow in a spiral microchannel. To achieve this, they designed a 5-loop spiral microchannel with periodic expansion arrays on its outer wall which is shown in picture I of Fig. 7b. This configuration generates a vortex, which results in a lift force (F_V) acting on particles. The impact of this force and Dean drag force (F_D) on particle movement, depending on their size, is illustrated in Picture I of Fig. 7b. As shown in Fig. 7b, the study focused on separating 6-, 10-, and 20-micron particles using these channels. The vortex-induced lift force alters the inertial lift force (which is due to the rotational motion that the expansion arrays induce in the fluid flow), affecting particle migration along with Dean drag force. Smaller particles (6- and 10- μm particles) settle near the outer wall due to the dominant lift force and near the inner wall due to Dean drag force. Equilibrium positions depend on particle size in such a way that the focusing lines of 10 μm particles are closer to the channel centerline than 6 μm particles. Larger particles (20 microns) reach equilibrium at the center of the channel, allowing steady separation at different fluid flow rates (in the range of 400 to 1000 $\mu l/\min$). The final focusing lines of all particles are illustrated in picture I of Fig. 7b. The chip was tested for separating Circulating Tumour Cells (CTCs) from blood cells, effectively focusing cells within the channel. The experimental results depicted in picture II of Fig. 7b demonstrate the recovery rates of three distinct types of Circulating Tumour Cells (CTCs), revealing that these CTCs can be effectively recovered at a high percentage. However, as shown in picture III of Fig. 7b, achieving desired purities for CTCs was challenging due to their sizes being close to white blood cells (WBCs) [61]. Although the proposed microchannels by Gou et al. [61] and Shen et al. [60] achieved at a high focusing efficiency of particles or cells within a certain range of flow rates, it seems that the proposed geometry of the microchannel creates more than single stream focusing line and affected adversely on the purity of cell separation. Therefore, more efforts on the improving of the geometry of the spiral microchannels combined with expansion arrays is demanded. In 2020, Erdem et al. [62] introduced elliptic configurations in spiral microchannels to counter linear radius increase issues. The study used microchannels with same width and height but different initial aspect ratios (IARs) of 3:2, 11:9, 9:11, and 2:3 to adjust the curvature radius which are shown in Fig. 7c. IAR refers to the ratio of r_x to r_y is these parameters are determined in Fig. 7c. The elliptical loops of the spiral microchannel affect the Dean drag force along each quarter loop compared to conventional spiral microchannel. The variation of the Dean velocities distribution at the beginning and at the end of the last quarter loop of the channel with all IARs is shown in Fig. 7c. Results indicated that above a critical Reynolds number (for each microchannel type), around flow rates of 3.0 to 3.1 $ml/\min$, the separation sensitivity increased. 20-μm particles concentrated near the inner wall due to inertial lift force dominating over Dean drag force, while 10-μm particles migrated towards the centerline due to the Dean drag force effect. Achieving purity over 90% for 20-μm particles and 85% for 10-μm particles was possible with the microchannel having an IAR of 3:2. Channels with IARs above one showed higher separation purity compared to those with IARs below one. This is due to decreased curvature radius in the last loop quadrant, intensifying Dean drag force and widening the particle focus line which can be found by Fig. 7c. Erdem et al. proposed a spiral microchannel design that alters Dean flow intensity in loops, suitable for binary separation. The close alignment of particle focus lines impacts separation purity [62]. In 2022, Gangadhar and Vanapalli [63] studied the effect of adding turns to spiral arcs on Dean flows in a microfluidic Labyrinth device. The device has 11 loops and 56 corners and shown schematically in Fig. 7d. They investigated particle and cell focusing dynamics under various flow rates and Reynolds numbers. U-shaped turns and non-monotonic curvature inside the device generate circulatory forces influencing particle focusing differently from spiral microchannels. Cell focusing was found to be less impacted by sharp turns than particle focusing. The study indicates that turn size and flow conditions can either enhance or diminish particle separation. Sharp turns alter the direction of cross-sectional flow, affecting particle streak width, which may not always benefit particle focusing [63]. In 2023, Ebrahimi et al. [64] conducted a study on a curved contraction-expansion (CEA) microchannel for filtering circulating tumour cells (CTCs) from white blood cells (WBCs). The general schematic of the curved CEA microchannel proposed by this group is presented in picture I of Fig. 7e. The channel design incorporated expansion zones to enhance separation efficiency, decrease processing time, and reduce costs for achieving higher purity and efficiency in cell separation compared to conventional straight CEA channels. As picture II of Fig. 7e shows, their research showed an 11.48% increase in efficiency compared to the straight-CEA microchannel design. But, formation of vortices inside the expansion arrays is a vital

issue affected the separation efficiency and purity of the isolated cells providing using the proposed design by this group. The streamlines of the fluid, which reveal the vortices within the expansion arrays resulting from the computational analysis of the fluid flow, are depicted in picture III of Fig. 7e. Increasing the flow rate beyond 7.5 $ml/\min$ boosted the flow velocity so much that the cells couldn't pass through the expansion arrays [64]. The growth of vortices in the expansion arrays due to higher flow rates is another factor that prevents the passage of cells into the expansion arrays. Therefore, study on the shape of the expansion arrays which the formation of vortices within them is less possible should be followed.

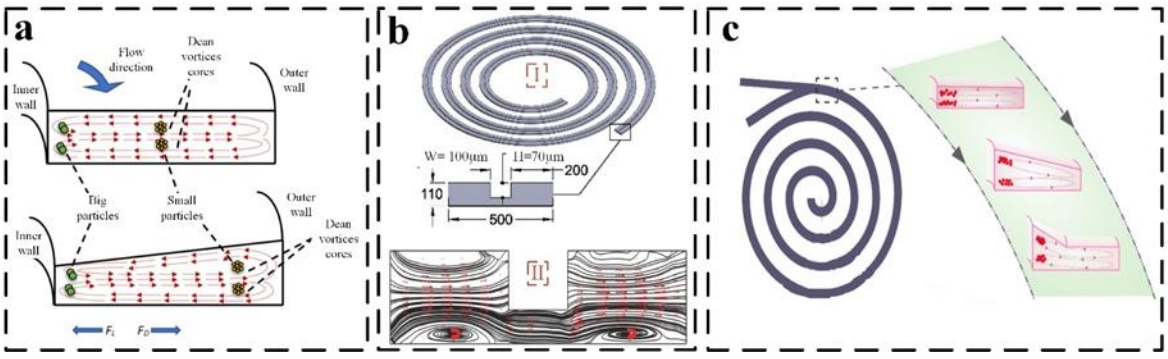

Fig 6. Effect of Cross-Section Shape on Dean Vortices and Particle Equilibrium Positions. a) A comparison of Dean vortices shape and particle equilibrium positions in trapezoidal and rectangular cross-sections [55]. b) Illustration of a spiral microchannel with a stair-like cross-section shown in pic. I by Ghadami et al. [56]. Streamlines across the stair-like cross-section are depicted in II. c) Schematic showing the influence of various cross-section shapes on Dean vortices and particle equilibrium positions [59].

The study results demonstrate that incorporating expansion arrays into spiral microchannels can significantly improve both separation efficiency and throughput concurrently. Altering the loop pattern of standard spiral microchannels proves to be less effective in controlling particle equilibrium compared to channels outfitted with expansion arrays. This inefficacy primarily stems from the manipulation of Dean flow, which closely follows particle trajectories. Introducing turns that do not induce secondary flows in the same direction adversely impacts particle focusing. Moreover, the incorporation of expansion regions into conventional spiral microchannels exerts a more pronounced influence on particle trajectories. In such instances, particles undergo accelerated motion upon exiting an expansion array, subjecting them to additional hydrodynamic forces. Consequently, particles tend to concentrate closer to the wall where the expansion arrays are situated. Consequently, particles' equilibrium positions exhibit greater predictability in conventional spiral geometries when combined with expansion arrays.

4. Design method of spiral microchannels

To optimize spiral microchannels, purposeful design is crucial. This section examines different design methods used for spiral microchannels. In 2009, Di Carlo [19] provided initial guidelines for straight microchannels but they have not been fully confirmed by experiments. Equation 7 estimated the required channel length for particle focusing based on lift force coefficient (in the range of 0.02 – 0.05), applicable to straight channels with specific aspect ratios (0.5 - 2) [19].

$$L_f = \pi\mu H^2 / \rho U_m a_p^2 f_L \tag{7}$$

$$Q = 2\pi\mu W H^3 / 3\rho L a_p^2 f_L \tag{8}$$

Additionally, Equation 8 estimates the necessary flow rate (Q) for particle focusing based on fluid velocity (U_m) and particle size (a_p) [19]. Di Carlo [19] also proposed a method for designing curved channels using the largest radius of curvature and smallest channel dimension to meet length and flow rate requirements. However, the relationship between channel design methodology and secondary flow intensity within the microchannel might need further investigation. Neglecting the impact of inertial migration velocity on particles in curved channels suggests a more comprehensive framework may be necessary for designing spiral microchannels. One study by Warkiani et al. [21] in 2015 proposed a focused design strategy to manipulate target cells or particles within these channels. They developed a spiral microchannel that effectively separates larger particles from smaller ones. The larger particles are the one that satisfy the criteria of $a_p/H \sim 0.1$ and can be focused, where a_p and H are the particle size and

channel height, respectively. In their method, the required length of the spiral channel is obtained based on the completing a Dean cycle by small particles (Equation 9). Equation (9) demonstrates that the time required for small particles to traverse the channel along its axis is equivalent to the time needed for these particles to complete one full cycle within the channel [21].

$$L_C = \left(U_f / U_D\right) L_{DC} \tag{9}$$

$$L_{DC} \approx 2W + H \tag{10}$$

where, U_f , U_D , L_{DC} , and W are the average flow velocity, laterally migration velocity of particles (obtained by Equation (2)), the length for one Dean cycle migration, and channel width, respectively. Gou et al., [61] in 2019 proposed a new spiral microchannel design integrating expansion arrays. In their design method, all of the particle sizes pass the criteria of $a_p / H > 0.07$ (a_p and H are particle size and channel height) and focus within the channel. Initially, they set the spiral radius to prevent chip collapse under high inlet pressure. Next, they calculate the loop numbers needed for particles to reach the focusing distance based on balance between lift and Dean drag forces, which there is more loops for smaller particles. The focusing distance is determined by Equation 11, involving fluid viscosity (μ), hydraulic diameter D_h), transverse migration distance (L_L), and inertial lift force coefficient (f_L) (f_L is generally assumed to be 0.5). The channel height is determined based on the smallest particle size using the relationship $a_p / H > 0.07$ [61].

$$L \geq 3\pi\mu D_h^2 L_L / 4\rho U_f a_p^3 f_L \tag{11}$$

The suggested methods for designing spiral microchannels are useful because they help researchers in determining the necessary channel length based on their objectives. However, these design approaches may not provide enough detail, which can make it tricky for researchers to gain a complete understanding of the best flow rates, particle equilibrium positions, ultimately resulting in an overestimation of the necessary channel length. These estimations are based on equations derived from assumptions. Consequently, researchers must subsequently evaluate the microchannel's performance through numerical simulations or experimental testing, necessitating a trial-and-error approach. This approach presents significant challenges, resulting in both high costs and time consumption.

4.1. Performance enhancement and optimization of spiral microchannels in Microfluidic Systems

Some researchers conducted studies to improve the performance of spiral microchannels in microfluidic systems. They aimed to enhance particle or cell sorting within the microchannels. Saha et al. [65] in 2007 optimized the dimensions of a microfluidic channel using computational fluid dynamics (CFD) to achieve fast particle separation. They tested different spiral geometries with varying cross-sectional heights, aiming to separate two particle types representing RBCs and WBCs. The chosen geometries had a single inlet, two outlets, and three spiral loops. By adjusting the dimensions of the model, they optimized the-sectional area of the microchannel for efficient particle separation with a constant flow rate. Several parameters were studied and optimized, including Reynolds number, aspect ratio, and geometric design manipulability. For one microchannel geometry, five simulations were performed with different inlet velocities (from 0.25 m/s to 0.55 m/s). These simulations helped determine an optimum inlet velocity for successful particle separation. After selecting an appropriate velocity value, two more simulations were conducted for different micro models with various cross-sectional heights. Simulations with higher inlet velocities (0.5 m/s - 0.55 m/s) exhibited better inertial particle focusing due to increased Reynolds number resulting in more distinct separation between heavy particles (WBCs) and light particles (RBCs). In contrast, lower inlet velocities led to spaced-out equilibrium where particles mixed without successful separation. Amongst tested heights, successful particle separation was achieved in a 135 μm -height microchannel while other channels resulted in mixed particle types at outlets. In this study, a two-way coupling between the fluid and the particles was not considered. The two-way coupling of particle–particle interaction was ignored, and the particles were assumed to be non-deforming [65]. In a study by Kim et al. [66] (2014), they looked at how changing the curvature of spiral microchannels affects the way cells are focused and separated. They designed multiple spiral microchannels with different curvatures (1250 – 5000 μm) and a fixed channel height and width of 50 and 200 μm . They used small plastic spheres labeled with fluorescence to see how the particles were focused. They observed the movement of the particles as the fluids flowed through the channels. They made sure the channels were long enough for complete focusing. They found that as the flow velocity increased, both 10 and 20 μm particles moved towards the center of the channel and then back to the wall. Larger particles took longer to move, so they stayed closer to the center. When the channel curvature increased, the movement of both particles decreased. This means that a higher flow velocity is needed for

optimal separation [66].

Therefore, to optimize and enhance the performance of a spiral microchannel, it is crucial to examine the effects of key parameters on particle trajectory. In both articles reviewed in this section, each parameter's effect was studied independently while holding the other parameters constant. The studies on binary separation indicated that higher fluid flow rates improved separation efficiency. Additionally, a larger curvature radius of the microchannel had a detrimental impact on particle separation due to the weakening of the Dean vortices. Overall, it is evident from the articles that the optimal conditions for each spiral microchannel are determined by considering factors such as the microchannel's geometry (including dimensions such as channel width, height, length, and curvature radius), cross-sectional shape, and particle size. It is important to note that optimizing the performance and dimensions of spiral microchannels is unique to each specific geometry and cross-sectional shape.

5. Advancements in Fabrication Techniques and Their Impact on Particle Manipulation in Microfluidic Systems

The fabrication of microchannels is a crucial factor in the advancement of microfluidic devices. Over the years, various fabrication techniques have been developed and used for a wide range of applications and materials. Depending on the specific use of microchannel-based devices, different materials are preferred. To meet the growing demand for these devices, hybrid techniques have also been developed to manufacture microchannels efficiently.

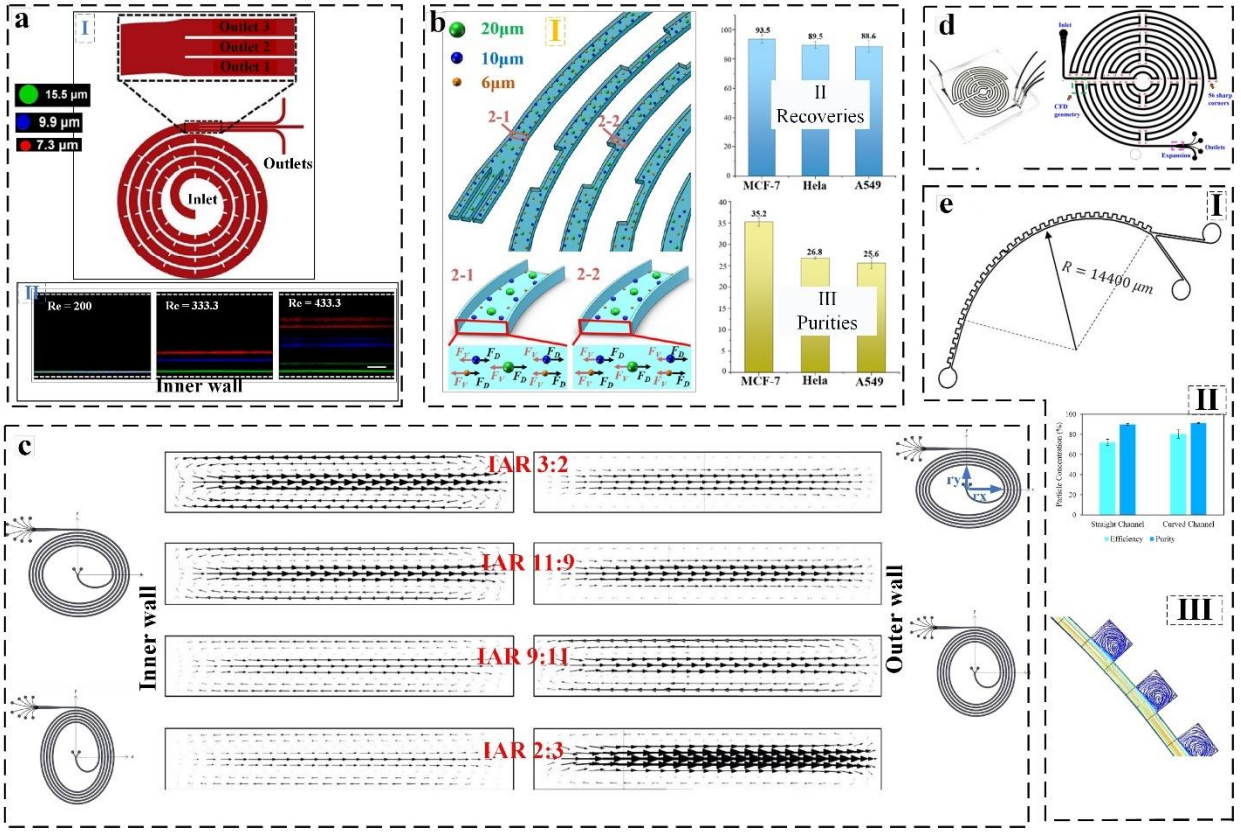

Fig 7. The effect of loop patterns and microchannel geometry on Dean vortices and particle equilibrium positions. a) Shows the innovative design (I) of a spiral microchannel with micro-bars proposed by Shen's group [60], with fluorescent images (II) capturing particle trajectories of varying diameters (15.5 μm , 9.9 μm , and 7.3 μm) at different flow rates (Re =300, 333.3, and 433.3). b) Demonstrates particle behaviour (I) in a spiral microchannel featuring expansion array on its outer wall by Gou's group [61], along with the recoveries (II) and purities (III) of MCF-7, Hela, and A549 cells from experimental tests. c) Illustrates schematics of elliptic spiral microchannels with different aspect ratios (IARs of 3:2, 11:9, 9:11, and 2:3) and highlights the variation of Dean vortices along the channel length [62]. d) Introduces the labyrinth device geometry proposed by Gangadhar's group [63]. e) Compares the efficiency and purity (II) of straight and curved CEA (curved-CEA, I) microchannels in separating MCF-7 cells from L929 cells, showcasing streamlines (III) obtained from numerical calculations in the expansion arrays of a curved CEA-microchannel [64]

Table 1. Summary of the results obtained from parameter study.

Target parameter	Research group	Microchannel characteristics	Results	Drawbacks	Discrepancies
Particle size	Bhagat et al. [48]	- 5-loop spiral microchannel; - Two inlets and Two outlets; - 100-micron width; - 50-micron height.	- Binary separation between two different sized particles/cells was examined. - Larger particles focused close to the inner wall of the channel; due to inertial lift force over Dean vortices. - Smaller particles or cells got trapped into the Dean cycles. - Particles or cells that pass the criteria of ($a_p/H > 0.07$) are focused within the spiral microchannels.	The separation sensitivity and efficiency of the cells or particles are highly dependent on the fluid flow rate.	-
	Warkiani et al. [21]	- 2-loop spiral microchannel; - Two inlets and Two outlets; - 500-micron width; - 170-micron height; - Three stacked chip.			
	Yoon et al. [49]	- A half-loop curved channel; - Two inlets and two outlets; - 150-micron width; - 75-micron height.	- The binary separation of particles which pass the criteria of ($a_p/H > 0.07$) was examined. - At normalized heights of 0.27 and 0.72, zero velocities consistently occur, leading to size-selective separation. - The larger particles which their size is as ($a_p/H > 0.27$), focused close to the outer wall. - The smaller particles ($a_p/H < 0.27$), focused near the inner wall.	-	
	Guzniczak et al. [50]	- Six-loops; - 170-micron width; - 30-micron height.	Large cells with $a_p/H > 0.27$ focused close to the outer wall of the spiral microchannel	-	

Aspect ratio	Kuntaegowdanahalli et al. [11]	- A 5-loop Archimedean spiral microchannel; - 500-micron width; - Varied height, 90-140 microns; - Two inlets and eight outlets.	- The equilibrium positions of single sized particles were examined in channels of varying heights and De . - For each channel height, by increasing the flow rate, De increased and the stream line of the focused particles got away from the inner wall. (due to the dominance of the Dean drag force over the inertial lift force). - At an approximate constant flow rate, De stayed approximately constant and by increasing the channel height, the stream line of the focused particles got closer to the channel center.	-	According to both articles, increasing the channel's height and width in spiral microchannels makes the effect of Dean vortices on the particles' equilibrium position more dominant than the inertial lift forces. When the channel height increases, stronger Dean vortices move the stream of particles closer to the channel center, while increasing the channel width moves the particles closer to the channel's inner wall.
	Martel and Toner [51]	- A 2.5-loop spiral microchannel; - Constant channel height of 50 microns; - Varied channel width of 50 microns to 400 microns.	- Wider spiral microchannels have a more flattened flow field, lower shear gradient, at constant fluid velocity. - Wider channels experience a stronger Dean drag force on particles, causing the particles to be focused closer to the inner wall.	-	
	Nivedita et al. [52]	- Three 2.5-loop Archimedean spiral microchannels with three different aspect ratios of: (150×250 micron), (100×250 micron), (100×500 micron) as (height × width).	- Under a critical Dean number (De_c), only two counter-rotating Dean vortices were formed, while more than two vortices appeared beyond this critical value. - De_c is highly influenced by the AR , where $AR = \frac{H}{W}$. ($De_c \propto AR^{-0.5}$)	-	-

	Cruz and Hjort [53]	- Two-loop spiral microchannel; - 6.15-micron width; - 14.5-micron height; - One inlet; - Three outlets.	In the described study, it has been reported that the HARC systems (H>H) possess the ability to not only separate particles but also achieve this with incredibly high precision. The researchers demonstrated this capability for particles differing in size by as little as 80 nm.	Only the separation of sub-micron particles was studied in spiral microchannels with high aspect ratio.	-
Cross-section shape	Al-Halhouli et al. [55]	- Trapezoidal cross-section spiral microchannel; - 8-loop spiral microchannel; - 600-micron width; - Inner/outer heights of 50 and 90 microns.	- Trapezoidal spiral channels, in contrast to rectangular channels, generate Dean vortices with cores shifted towards the outer wall. This causes small particles to be positioned differently, leading to improved separation efficiency. - High-throughput (>1 ml/min) and high-resolution binary separation	- Cost and accessibility of fabrication method	
	Ghadami et al. [56]	- Stair-like cross-section; - 4-loop spiral microchannel; - 500-micron width; - 110-micron height; - 40-micron height for middle section;	- Contrary to traditional spiral microchannels, vortices are sequentially formed across the cross-section. - At flow rates ranging from 2000 to 2304 microliters per minute, the binary separation took place, demonstrating high-throughput separation. - higher separation sensitivity than traditional spiral microchannels.		
	Mihandoust et al. [59]	- Complex cross-section of trapezoidal and rectangular cross-sections; - 4.5-loop spiral microchannels; - Total width of the channels was 400-, 500-, and 600- microns;	- Overcoming the challenge of focusing particles that do not meet the ($a_p/H > 0.07$) criteria. - A 500-time increase in sample concentration in the 600		

		- Inner and outer heights in all channels were 100- and 40- microns.	μm channel from the inlet concentration		
Loop pattern	Shen et al. [60]	-4-loop spiral microchannel combined with ordered micro-obstacle; -Total channel width of 900 microns; -Obstacle length of 450 microns; -Channel height of 100 microns.	- The particles concentrated near the inner wall where the obstacles were placed. - Particle concentration occurred at flow rates exceeding 3 ml/min. - As the flow rate increases, particles separate, with smaller ones moving closer to the outer wall of the channel.	Higher flow rates like 6.5 ml/min resulted in improved particle separation but risked splitting the stream into doubles due to high Reynolds number flow in the channel.	There was no consensus among researchers regarding the forces influencing the movement of particles in spiral microchannels with variable widths.
	Gou et al. [61]	-5-loop spiral microchannel combined with expansion structures; -75-micron height; -The width of narrow sections is 150 microns; -The width of wide sections is 300 microns.	-The stream line of the equilibrium position of larger cells or particles is at the center of the channel. -The smaller cells or particles focused on both sides of the channels -The focusing position of particles of all sizes remains independent of the fluid flow rate within the range of 400 to 1000 $\mu l/\text{min}$.	Cell separation occurred with low purities.	
	Ebrahimi et al. [64]	-A curved expansion-contraction microfluidic structure; -The width of the expansion array if 400 microns; -The width of the narrow sections is 200 microns.	- The CTCs focused close to the wall that the expansion arrays are placed on it (outer wall). - The smaller cells focused near the inner wall.		

These microchannels are typically fabricated on polymeric, glass, silicon, and metallic substrates. Polymeric and glass substrates are commonly utilized in biomedical and chemical devices, while silicon-based and metallic substrates are more common in electronic and mechanical engineering applications. However, large-scale fabrication of microchannels on these substrates has been challenging due to the precision required. The lack of suitable technologies for this process has impeded the further development of microchannel-based devices. Therefore, there is a need to explore new methods for faster and more cost-effective production of these devices to ensure sustainable development in this field [67].

In the field of microfluidics, the selection of an appropriate material for device fabrication is of utmost importance [68]. Several crucial factors must be taken into consideration, including wetting and contact angles, durability, ease of fabrication, transparency, biocompatibility, chemical compatibility, temperature and pressure resistance, as well as surface functionalization potential [68-71]. Many materials can be used for fabricating microfluidic devices, including glass, silicon, metals, polymers, and ceramics. The diversity and quality of these materials are continuously increasing. Each material has its own advantages and disadvantages, depending on its intended use [72].

- **Materials:**

Metals: Metals, such as aluminum, copper, and iron, have qualities that make them suitable for microchip fabrication. They are cheap, widely accessible, easy to machine, and can withstand high heat loads, high pressure, and toxic chemicals (except strong acids). Their resistance to robust handling is also convenient for cleaning operations. Metal-based microfluidic devices have been proven useful in nanomaterial synthesis, such as obtaining size-tunable methacrylic nanoparticles in a stainless-steel multi-lamination micromixer [73-75].

Silicon: Silicon is a popular choice for microfluidic systems due to its availability, chemical compatibility, and thermostability. However, it has limitations, such as opacity for optical detection, fragility, high elastic modulus, and relatively high cost [76]. Nonetheless, silicon microfluidic platforms are used in biological applications, such as point-of-care medical diagnostics and organ-on-chip devices for drug toxicity screening [77].

Glass: Glass is chemically inert, thermostable, electrically insulating, rigid, biologically compatible, and allows easy surface functionalization. These properties make glass-based microreactors suitable for carrying out chemical reactions that require extreme conditions such as high temperatures, high pressures, and aggressive solvents. The higher resolution at the micrometer scale that is achieved in glass microcapillary reactors compared with other materials makes these devices suitable for the better-controlled synthesis of emulsions and polymeric nanoparticles. Glass also has the advantages of excellent optical transparency, a lower price, and the possibility of integrating active components. Not only valves and pumps of other materials can be employed in such chips, but the glass itself can be integrated as an active component in the form of ultra-thin glass sheets. Due to its transparency, glass can be used for optical detection. Additionally, the glass's thermal and chemical stability allows for the effective cleaning of the device once the experiment is over, either by heating the chip or washing it with chemicals. Glass compatibility with biological samples makes it useful for biochemical analyses. Hence, it is no surprise that glass is one of the most popular materials for microfluidic chips. In terms of composition, these substrates are usually made of soda-lime glass, borosilicate glass, and fused quartz [72].

PDMS: However, microfabrication difficulties arise, limiting the applications of glass microfluidic devices. One of the most representative materials of this class is PDMS, an elastomer with excellent microchip fabrication properties. Owing to its properties, PDMS is valuable for bio-related research, such as long-term cell-culture, cell screening, and biochemical assays. PDMS microdevices can detect bacteria, as well as their proteins and DNA, which is highly useful for disease diagnosis. Thin membranes made of PDMS can also be used for valves and pumps. However, the same properties become obstacles in organic synthesis. The porosity of PDMS makes it an adsorptive material, in which many molecules can diffuse. This renders the material incompatible with organic solvents, as their molecules can be adsorbed into channel walls and swell the platform. Another issue may arise from water evaporation through channel walls, which leads to a change in the concentration of a solution. To overcome these problems, other polymeric materials are being investigated for microfluidic fabrication, depending on desired properties and final application [68, 74, 77, 78].

PMMA and perfluorinated polymers: Two materials commonly used for microchip manufacturing are PMMA and perfluorinated polymers. PMMA, an amorphous thermoplastic, shows better solvent compatibility than PDMS and no small-molecule absorption. It is optically transparent, possesses good mechanical properties, allows surface modification, and supports prototyping at a small scale of production. These properties make it particularly useful

for organ-on-a-chip devices and micro-physiological systems. Perfluorinated polymers, such as Teflon PFA, Teflon FEP, and PTFE, feature thermo-processability, chemical inertness, organic solvent compatibility, and excellent antifouling properties. Additionally, they provide optical transparency, moderate gas permeability, and sufficient flexibility to make diaphragm valves. These materials are recommended for applications in cell cultures, high-precision assays, super-clean tools, and valve and pump fabrications. PTFE, specifically, is suitable for synthesis devices due to its tolerance to various chemicals and high temperatures, as well as its resistance to channel blockage from aqueous solutions thanks to its hydrophobic nature. However, the availability of fluoropolymer microdevices is limited due to challenges with micropatterning and elasticity [76, 77, 79, 80].

TEs: Macromolecular compounds called TEs, composed of two monomers, each with at least two thiols or allyl (or ene) groups, offer higher solvent resistance than PDMS, PMMA, and COCs, along with enhanced optical transparency in the visible spectrum, but their UV transmittance depends on composition [70].

Epoxy resins: Epoxy resins, used in microfluidic device fabrication, are known for stability at high temperatures, chemical resistance, transparency, and high resolution, but their main drawback is the high cost [81, 82].

Hydrogels: Hydrogels, porous networks of hydrophilic polymer chains, boast biocompatibility, low cytotoxicity, biodegradability, controllable pore size, high permeability, and an aqueous nature, making them ideal for various biomedical applications. However, their main limitation lies in maintaining device integrity in the long term [76, 77, 83].

The mentioned materials can be combined to create hybrid devices for synergistic utilization. Possible approaches include placing soft films between hard chips to form diaphragm valves, incorporating channels with metal electrode-patterned substrates, combining materials to adjust channel permeability, or implanting photocurable materials to create in situ structures [76]. Koijc et al. [84] in 2019, proposed a composite microfluidic device using PVC foils and Ceram Tapes, demonstrating good optical, mechanical, and thermal characteristics, as well as resistance to high flow rates. Gao et al. [85] in 2019 developed a hybrid device combining gas-permeable PDMS with NOA81 to control oxygen tension in microfluidic cell cultures. Chen et al. investigated glass–PDMS–glass sandwich configurations for microfluidic devices, providing the advantage of dismounting and reusing them for various applications.

There are various materials available for fabricating microfluidic devices, each with different properties and behaviors during processing. Fabrication methods must be tailored to the specific material characteristics and production needs. Cost is also a crucial factor, especially considering that microfluidic platforms are often disposable. Therefore, the chosen method should be economically feasible for one-time-only chips. Additionally, for widespread adoption, chips should be produced in an accessible and scalable manner. The classification followed here categorizes fabrication methods based on the processes involved, such as chemical, mechanical, laser-based, and others [72].

- **Fabrication methods**

Chemical Processes: The most commonly utilized techniques include wet and dry etching. Wet etching has gained popularity due to its fast-etching rate and the ability to process a large quantity of wafers simultaneously [86]. However, this technique requires strong chemicals, with hydrofluoric acid being the usual etchant of choice [87]. This limitation poses significant safety and environmental hazards due to the highly corrosive nature of the etchants [88]. In contrast, dry etching techniques, such as reactive ion etching, offer solutions to some of the challenges associated with wet etching. These methods enable the creation of precise microscale channel profiles due to the directional nature of ion bombardment [86]. Dry etching is recommended for transparent substrates but is generally not preferred due to its slower rates compared to wet etching and poor selectivity relative to the mask [87].

Mechanical Processes: The first known method for fabricating microfluidic devices, micromachining, was originally used in the semiconductor field [88]. To ensure crack-free surfaces, good dimensional accuracy, and surface roughness, mechanical processes are crucial [86]. While suitable for silicon, glass, and polymer-based devices, these techniques can be used to create replication masters [89, 90]. Mechanical cutting, abrasive jet machining, and ultrasonic machining offer cost-effectiveness and flexibility, enabling the creation of complex 3D structures when used in combination with other processes [86]. However, mechanical fabrication processes have lower precision and productivity compared to lithographic methods [86]. Micro-milling, utilizing high-precision computer numerical controlled motion, is an effective and economical method for creating complex 3D structures [86, 91, 92]. Abrasive air-jet machining and abrasive water-jet machining are nontraditional methods that allow for precise fabrication of complex parts [86, 93]; the latter benefits from the high viscosity of water, providing better jet characteristics [86].

Injection molding is a widely used method for processing polymers for everyday objects due to its high throughput, cost efficiency, and precision [89]. This method has also garnered attention in microfluidics fabrication, often referred to as micro-injection molding. The process involves transferring pre-polymerized pellets of a thermoplastic from a hopper into a heated barrel, melting the material, injecting it under pressure into a heated mold cavity, and then releasing the solidified material from the mold [89, 94]. However, micro-injection molding has limitations such as material restrictions to thermoplastics and mold issues related to expensive fabrication and limited resolution [95].

Hot embossing, similar to injection molding, relies on melting thermoplastics and shaping them into molds using pressure and heat [95]. In contrast to injection molding, the material is poured and pressed against the mold to transfer the desired features from the cast to the softened polymer, reducing stress and allowing for more delicate designs. Nonetheless, hot embossing shares the limitation of being applicable only to thermoplastics [95].

Soft lithography, also known as "replica molding," is a popular method for making biomedical microfluidic devices [91, 95]. It involves creating a hard master, pouring liquid polymer into the mold, heat-curing, and peeling off the polymer to produce a flexible cast-molded stamp for printing, molding, and embossing micro- and nanostructures [72, 91]. This approach offers high-resolution replicas, lower costs, and faster production compared to photolithography. It also enables the generation of intricate 3D flows and pneumatic control lines, as well as the production of highly flexible and optically transparent designs [95-97]. However, limitations include possible pattern deformation during cast removal and the need for costly photolithography techniques to create the hard master [95, 96].

Laser-Based Processes: Lasers are relatively affordable for fabrication when compared to cleanroom facility costs and are generally expensive tools [91]. Laser ablation enables quick and flexible generation of microfluidic patterns on various materials without the risks of chemical fabrication methods [88, 98]. The working principle involves optical amplification of light through stimulated emission of electromagnetic radiation [86], resulting in thermal degradation that engraves microstructures on the material's surface [91]. Short-duration laser pulses break chemical bonds from polymer molecules, leading to the ejection of decomposed polymer fragments and the creation of photo-ablated cavities [90, 99]. However, drawbacks include weak reproducibility due to poor laser focusing control, unwanted surface effects, limited throughput, and variations in product quality among different types of lasers [72, 99].

Three-Dimensional printing: Three-dimensional printing has revolutionized the creation of microfluidic channels, offering precise material application and diverse chip designs for complex microfluidic structures. Various manufacturing technologies, like fused deposition modeling, inkjet printing, and multi-jet printing, have harnessed the benefits of 3D printing [72, 100].

While these technologies have advantages, limitations persist, including low z-resolution, restricted transparent materials, the need for smooth surface finishes, and challenges in fabricating hollow and void sections [100].

Fused deposition modeling, a widely used 3D printing technology, allows for simple, effective, and affordable multi-material printing. However, it faces issues such as compressive stress fractures and filament size mismatches with microfluidic channels [72].

Multi-jet modeling, or PolyJet, offers high accuracy and the ability to create multi-material microfluidic platforms. Inkjet printing, known for depositing a variety of materials, has emerged as a low-cost and precise method for chip production [72].

In the preceding sections, we explored various techniques for fabricating microfluidic chips, delving into their respective strengths and limitations. Notably, soft-lithography and three-dimensional printing stand out as non-traditional, advanced methods compared to others, and have become the predominant approaches for microfluidic chip production. In the realm of microfluidic chip fabrication, the utilization of 3D printing technology presents a promising avenue for advancement. Existing 3D printers, however, present limitations in their capability to produce chips with uniformly integrated holes and microchannels. Consequently, the development of a 3D printing method with the capacity to consistently fabricate chips featuring uniform microchannels of desired dimensions constitutes an opportunity to realize cost-effective chip production. Such an advancement would alleviate the challenges associated with accessing clean room facilities and the need for precise laser equipment.

Hybrid technologies emerged as a way to address the challenges and limitations of individual fabrication methods. For example, Alapan et al. [101] combined 3D printing with micromachined laser lamination to produce intricate transparent microfluidic devices, eliminating the need for costly and time-consuming cleanrooms while enhancing the precision of the lamination process.

6. Conclusions and Outlook

In this review, we explore spiral microchannels for particle separation by emphasizing their unique advantages over straight microchannels. Spiral microchannels offer a single equilibrium position for particles, unlike straight ones that can create multiple equilibrium points. The geometrical features of spiral microchannels lead to higher separation efficiency. Research indicates that in the case of straight microchannels, particle equilibrium is influenced by shear gradient lift force and wall-induced lift force. However, the introduction of Dean drag force in spiral microchannels alters the equilibrium and reduces focusing lines. Both lift and Dean drag forces rely on factors like fluid flow rate, microchannel dimensions, and particle size. Therefore, in the present work, the effects of different vital parameters, including particle size and channel dimensions, are fundamentally discussed. We specifically explore how cross-sectional shape and loop pattern of spiral microchannels influence the intensity, shape, and position of Dean vortices, based on previous studies. The major difference between this work and other article is our examination of how Dean vortices affect particle equilibrium positions. This understanding enables the intelligent design of spiral microchannels.

Changes in geometric and operational parameters significantly affect Dean flow and inertial forces, subsequently impacting particle equilibrium. This review aims to analyse the specific influence of these parameters on particle equilibrium in spiral microchannels. The studies on the impacts of particle size and spiral microchannel aspect ratio on the equilibrium position of particles is summarized as follows:

- Only particles meeting size criterion ($a_p/H > 0.07$) can focus through the spiral microchannel. Larger particles ($a_p > 0.27H$) concentrate towards the outer channel wall.

- In a low aspect ratio spiral microchannel, reducing the aspect ratio brings particles closer to the inner wall. Higher flow rates move particles towards the channel center when dimensions remain constant. The dimensionless number of De_c determines secondary Dean vortex presence, affecting particle focusing.

In conventional spiral microchannels with rectangular cross-sections, the strength of the Dean vortices reduces as the curvature radius gets larger, impacting the separation of particles with varying sizes. To address this issue, scientists have studied the influence of two factors: the shape of the cross-section and the pattern of loops in the spiral microchannels. Here are the findings from their research:

- Choosing the right cross-sectional shape of spiral microchannels is a key for purposeful particle positioning. Rectangular sections are simple to make and predict particle positions but lack vortex control. Trapezoidal sections enable efficient separation, but challenges in fabrication may increase costs. Complex geometries for channel cross-section can enhance vortex control and allow for high-throughput separations but are harder to fabricate. Precise control over the shape of vortices is still challenging.

- Adding expansion arrays to spiral microchannels boosts separation efficiency and throughput. Changing the loop pattern of standard spirals is less effective in controlling particle equilibrium. Expansion arrays in spiral microchannels have a stronger impact on particle trajectories, accelerating particle motion and concentrating particles closer to the wall. Consequently, particles show more predictable equilibrium positions in conventional spirals with expansion arrays.

To design conventional spiral microchannels, researchers typically employ three design methods, usually focusing on two of them. These methods prompt the consideration of whether particles of varying sizes can be accurately focused. When aiming to focus all particles, the design must find a compromise between the Dean drag force and lift force, particularly for the smallest particles. If the objective shifts to focusing solely on the largest particles (those meeting the criteria of $a_p/H > 0.07$), the smaller particles become trapped in the Dean flow. Consequently, in the latter scenario, the channel's necessary length is determined by equating the time needed for small particles to traverse the channel along its axis with the time required for these particles to complete one full cycle within the channel.

Predicting the magnitude and direction of the inertial lift force on particles is crucial in modelling their trajectory in spiral microchannels. Researchers have developed various models to calculate the inertial lift force components tailored to specific conditions. for 3D models, initially, coefficients for straight microchannels with rectangular cross-section are determined. Subsequently, a coordinate transformation is carried out to align the lift force components onto a spiral geometry. Many studies focus on using spiral devices to separate particles or cells, but there is still a need to enhance these chips to achieve high separation efficiency and purity, separate particles of varying sizes, improve chip lifespan, and address fabrication challenges. Future research on hybrid geometries of spiral devices shows promise in maximizing efficiency and purity while reducing costs. This involves exploring complex cross-sections and loop pattern modifications studied in the past. Despite previous efforts, researchers have

not determined the optimal shape and intensity of Dean vortices that would be most effective in achieving their separation goals. Advancements in understanding and controlling Dean vortices in spiral devices could lead to significant improvements in particle separation techniques.

It is suggested that to achieve specific goals such as separating particles of different sizes and improving the sensitivity of separation between two focusing lines, researchers should first determine the desired strength and pattern of Dean vortices. Subsequently, they should design the shape and layout of the spiral microchannel based on the characteristics of the Dean vortices. Lastly, the efficiency of the microchannel in separating particles or cells can be predicted by simulating its performance. To study how different factors like cross-sectional dimensions and shape, number and length of spiral microchannel loop, expansion array features, and flow rate influence the position of particles in microchannels, it is proposed to develop an artificial intelligence algorithm. This algorithm can accurately predict how these factors affect particle equilibrium. Such research can advance our understanding of particle behavior in microchannels and contribute to the development of more effective microfluidic systems. Another crucial factor influencing the performance of microfluidic chips is the fabrication method. While many past studies have utilized lithography to produce their microfluidic devices, this approach may not be suitable for high-pressure microchannels or those with non-rectangular cross-sections. It is suggested that investigating alternative fabrication techniques, particularly 3D printing methods, can validate the chip's durability. Additionally, exploring suitable resins for integrated chip production can prevent leakage, especially in high-pressure drop scenarios.

References

[1] D. R. Gossett, W. M. Weaver, A. J. Mach, S. C. Hur, H. T. K. Tse, W. Lee, H. Amini, D. Di Carlo, Label-free cell separation and sorting in microfluidic systems, *Analytical and bioanalytical chemistry*, Vol. 397, pp. 3249-3267, 2010.

[2] J. Nilsson, M. Evander, B. Hammarström, T. Laurell, Review of cell and particle trapping in microfluidic systems, *Analytica chimica acta*, Vol. 649, No. 2, pp. 141-157, 2009.

[3] P. S. Dittrich, A. Manz, Lab-on-a-chip: microfluidics in drug discovery, *Nature reviews Drug discovery*, Vol. 5, No. 3, pp. 210-218, 2006.

[4] A. Shenoy, C. V. Rao, C. M. Schroeder, Stokes trap for multiplexed particle manipulation and assembly using fluidics, *Proceedings of the National Academy of Sciences*, Vol. 113, No. 15, pp. 3976-3981, 2016.

[5] F. Guo, Z. Mao, Y. Chen, Z. Xie, J. P. Lata, P. Li, L. Ren, J. Liu, J. Yang, M. Dao, Three-dimensional manipulation of single cells using surface acoustic waves, *Proceedings of the National Academy of Sciences*, Vol. 113, No. 6, pp. 1522-1527, 2016.

[6] M. Rafeie, J. Zhang, M. Asadnia, W. Li, M. E. Warkiani, Multiplexing slanted spiral microchannels for ultra-fast blood plasma separation, *Lab on a Chip*, Vol. 16, No. 15, pp. 2791-2802, 2016.

[7] A. F. Sarioglu, N. Aceto, N. Kojic, M. C. Donaldson, M. Zeinali, B. Hamza, A. Engstrom, H. Zhu, T. K. Sundaresan, D. T. Miyamoto, A microfluidic device for label-free, physical capture of circulating tumor cell clusters, *Nature methods*, Vol. 12, No. 7, pp. 685-691, 2015.

[8] Q. Zhao, D. Yuan, J. Zhang, W. Li, A review of secondary flow in inertial microfluidics, *Micromachines*, Vol. 11, No. 5, pp. 461, 2020.

[9] A. Najafpour, K. Hosseinzadeh, J. R. Kermani, A. Ranjbar, D. Ganji, Numerical study on the impact of geometrical parameters and employing ternary hybrid nanofluid on the hydrothermal performance of mini-channel heat sink, *Journal of Molecular Liquids*, Vol. 393, pp. 123616, 2024.

[10] M. Toner, D. Irimia, Blood-on-a-chip, *Annu. Rev. Biomed. Eng.*, Vol. 7, No. 1, pp. 77-103, 2005.

[11] S. S. Kuntaegowdanahalli, A. A. S. Bhagat, G. Kumar, I. Papautsky, Inertial microfluidics for continuous particle separation in spiral microchannels, *Lab on a Chip*, Vol. 9, No. 20, pp. 2973-2980, 2009.

[12] M. Kersaudy-Kerhoas, R. Dhariwal, M. Desmulliez, Recent advances in microparticle continuous separation, *IET nanobiotechnology*, Vol. 2, No. 1, pp. 1-13, 2008.

[13] Z. Wu, K. Hjort, G. Wicher, Å. Fex Svenningsen, Microfluidic high viability neural cell separation using viscoelastically tuned hydrodynamic spreading, *Biomedical microdevices*, Vol. 10, pp. 631-638, 2008.

[14] E. Hedlund, J. Pruszak, A. Ferree, A. Viñuela, S. Hong, O. Isacson, K.-S. Kim, Selection of embryonic stem cell-derived enhanced green fluorescent protein-positive dopamine neurons using the tyrosine hydroxylase promoter is confounded by reporter gene expression in immature cell populations, *Stem Cells*, Vol. 25, No. 5, pp. 1126-1135, 2007.

[15] R. Nasiri, A. Shamloo, S. Ahadian, L. Amirifar, J. Akbari, M. J. Goudie, K. Lee, N. Ashammakhi, M. R. Dokmeci, D. Di Carlo, Microfluidic-based approaches in targeted cell/particle separation based on physical properties: fundamentals and applications, *Small*, Vol. 16, No. 29, pp. 2000171, 2020.

[16] E. K. Sackmann, A. L. Fulton, D. J. Beebe, The present and future role of microfluidics in biomedical research, *Nature*, Vol. 507, No. 7491, pp. 181-189, 2014.
[17] S. Zhang, Y. Wang, P. Onck, J. den Toonder, A concise review of microfluidic particle manipulation methods, *Microfluidics and Nanofluidics*, Vol. 24, No. 4, pp. 24, 2020.
[18] J. Hansson, J. M. Karlsson, T. Haraldsson, W. Van Der Wijngaart, A. Russom, Inertial particle focusing in parallel microfluidic channels for high-throughput filtration, in *Proceeding of*, IEEE, pp. 1777-1780.
[19] D. Di Carlo, Inertial microfluidics, *Lab on a Chip*, Vol. 9, No. 21, pp. 3038-3046, 2009.
[20] J. Zhang, S. Yan, D. Yuan, G. Alici, N.-T. Nguyen, M. E. Warkiani, W. Li, Fundamentals and applications of inertial microfluidics: A review, *Lab on a Chip*, Vol. 16, No. 1, pp. 10-34, 2016.
[21] M. E. Warkiani, B. L. Khoo, L. Wu, A. K. P. Tay, A. A. S. Bhagat, J. Han, C. T. Lim, Ultra-fast, label-free isolation of circulating tumor cells from blood using spiral microfluidics, *Nature protocols*, Vol. 11, No. 1, pp. 134-148, 2016.
[22] D. Jiang, C. Ni, W. Tang, D. Huang, N. Xiang, Inertial microfluidics in contraction–expansion microchannels: A review, *Biomicrofluidics*, Vol. 15, No. 4, 2021.
[23] A. J. Chung, A minireview on inertial microfluidics fundamentals: Inertial particle focusing and secondary flow, *BioChip Journal*, Vol. 13, No. 1, pp. 53-63, 2019.
[24] Y. Saffar, S. Kashanj, D. S. Nobes, R. Sabbagh, The physics and manipulation of Dean vortices in single- and two-phase flow in curved microchannels: A review, *Micromachines*, Vol. 14, No. 12, pp. 2202, 2023.
[25] J. Su, X. Chen, Y. Zhu, G. Hu, Machine learning assisted fast prediction of inertial lift in microchannels, *Lab on a Chip*, Vol. 21, No. 13, pp. 2544-2556, 2021.
[26] C. Liu, G. Hu, X. Jiang, J. Sun, Inertial focusing of spherical particles in rectangular microchannels over a wide range of Reynolds numbers, *Lab on a Chip*, Vol. 15, No. 4, pp. 1168-1177, 2015.
[27] N. Liu, C. Petchakup, H. M. Tay, K. H. H. Li, H. W. Hou, Spiral inertial microfluidics for cell separation and biomedical applications, *Applications of Microfluidic Systems in Biology and Medicine*, pp. 99-150, 2019.
[28] W. R. Dean, Fluid motion in a curved channel, *Proceedings of the Royal Society of London. Series A, Containing Papers of a Mathematical and Physical Character*, Vol. 121, No. 787, pp. 402-420, 1928.
[29] D. Farajpour, A review on the mechanics of inertial microfluidics, *Journal of Computational Applied Mechanics*, Vol. 52, No. 1, pp. 168-192, 2021.
[30] I. H. Karampelas, J. Gómez-Pastora, Novel approaches concerning the numerical modeling of particle and cell separation in microchannels: A review, *Processes*, Vol. 10, No. 6, pp. 1226, 2022.
[31] K. Hood, S. Kahkeshani, D. Di Carlo, M. Roper, Direct measurement of particle inertial migration in rectangular microchannels, *Lab on a Chip*, Vol. 16, No. 15, pp. 2840-2850, 2016.
[32] B. Ho, L. Leal, Migration of rigid spheres in a two-dimensional unidirectional shear flow of a second-order fluid, *Journal of Fluid Mechanics*, Vol. 76, No. 4, pp. 783-799, 1976.
[33] P. G. Saffman, The lift on a small sphere in a slow shear flow, *Journal of fluid mechanics*, Vol. 22, No. 2, pp. 385-400, 1965.
[34] C. K. Tam, W. A. Hyman, Transverse motion of an elastic sphere in a shear field, *Journal of Fluid Mechanics*, Vol. 59, No. 1, pp. 177-185, 1973.
[35] E. S. Asmolov, The inertial lift on a spherical particle in a plane Poiseuille flow at large channel Reynolds number, *Journal of fluid mechanics*, Vol. 381, pp. 63-87, 1999.
[36] D. Di Carlo, J. F. Edd, K. J. Humphry, H. A. Stone, M. Toner, Particle segregation and dynamics in confined flows, *Physical review letters*, Vol. 102, No. 9, pp. 094503, 2009.
[37] K. Hood, S. Lee, M. Roper, Inertial migration of a rigid sphere in three-dimensional Poiseuille flow, *Journal of Fluid Mechanics*, Vol. 765, pp. 452-479, 2015.
[38] J. Su, X. Zheng, G. Hu, New explicit formula for inertial lift in confined flows, *Physics of Fluids*, Vol. 35, No. 9, 2023.
[39] S. R. Bazaz, A. Mashhadian, A. Ehsani, S. C. Saha, T. Krüger, M. E. Warkiani, Computational inertial microfluidics: a review, *Lab on a Chip*, Vol. 20, No. 6, pp. 1023-1048, 2020.
[40] H. W. Hou, M. E. Warkiani, B. L. Khoo, Z. R. Li, R. A. Soo, D. S.-W. Tan, W.-T. Lim, J. Han, A. A. S. Bhagat, C. T. Lim, Isolation and retrieval of circulating tumor cells using centrifugal forces, *Scientific reports*, Vol. 3, No. 1, pp. 1259, 2013.
[41] H. Gaur, B. Khidhir, R. K. Manchiryal, Solution of structural mechanic's problems by machine learning, *International Journal of Hydromechatronics*, Vol. 5, No. 1, pp. 22-43, 2022.
[42] Y. Shi, Q. Shi, X. Cao, B. Li, X. Sun, D. K. Gerontitis, An advanced discrete-time RNN for handling discrete time-varying matrix inversion: Form model design to disturbance-suppression analysis, *CAAI Transactions on Intelligence Technology*, Vol. 8, No. 3, pp. 607-621, 2023.

[43] C. Shen, Q. Zheng, M. Shang, L. Zha, Y. Su, Using deep learning to recognize liquid–liquid flow patterns in microchannels, *AIChE Journal*, Vol. 66, No. 8, pp. e16260, 2020.
[44] M. Gheisari, F. Ebrahimzadeh, M. Rahimi, M. Moazzamigodarzi, Y. Liu, P. K. Dutta Pramanik, M. A. Heravi, A. Mehbodniya, M. Ghaderzadeh, M. R. Feylizadeh, Deep learning: Applications, architectures, models, tools, and frameworks: A comprehensive survey, *CAAI Transactions on Intelligence Technology*, Vol. 8, No. 3, pp. 581-606, 2023.
[45] C. Luo, KELL: A kernel-embedded local learning for data-intensive modeling, in *Proceeding of*, 38-44.
[46] B. Liu, W. Lu, Surrogate models in machine learning for computational stochastic multi-scale modelling in composite materials design, *International Journal of Hydromechatronics*, Vol. 5, No. 4, pp. 336-365, 2022.
[47] S. J. Raymond, D. J. Collins, R. O'Rorke, M. Tayebi, Y. Ai, J. Williams, A deep learning approach for designed diffraction-based acoustic patterning in microchannels, *Scientific reports*, Vol. 10, No. 1, pp. 8745, 2020.
[48] A. A. S. Bhagat, S. S. Kuntaegowdanahalli, I. Papautsky, Continuous particle separation in spiral microchannels using dean flows and differential migration, *Lab on a Chip*, Vol. 8, No. 11, pp. 1906-1914, 2008.
[49] D. H. Yoon, J. B. Ha, Y. K. Bahk, T. Arakawa, S. Shoji, J. S. Go, Size-selective separation of micro beads by utilizing secondary flow in a curved rectangular microchannel, *Lab on a Chip*, Vol. 9, No. 1, pp. 87-90, 2009.
[50] E. Guzniczak, T. Krüger, H. Bridle, M. Jimenez, Limitation of spiral microchannels for particle separation in heterogeneous mixtures: Impact of particles' size and deformability, *Biomicrofluidics*, Vol. 14, No. 4, 2020.
[51] J. M. Martel, M. Toner, Inertial focusing dynamics in spiral microchannels, *physics of fluids*, Vol. 24, No. 3, 2012.
[52] N. Nivedita, P. Ligrani, I. Papautsky, Dean flow dynamics in low-aspect ratio spiral microchannels, *Scientific Reports*, Vol. 7, No. 1, pp. 44072, 2017.
[53] J. Cruz, K. Hjort, High-resolution particle separation by inertial focusing in high aspect ratio curved microfluidics, *Scientific Reports*, Vol. 11, No. 1, pp. 13959, 2021.
[54] S. Ramya, S. P. Kumar, G. D. Ram, D. Lingaraja, A short review of spiral microfluidic devices with distinct cross-sectional geometries, *Microfluidics and Nanofluidics*, Vol. 26, No. 12, pp. 95, 2022.
[55] A. a. Al-Halhouli, W. Al-Faqheri, B. Alhamarneh, L. Hecht, A. Dietzel, Spiral microchannels with trapezoidal cross section fabricated by femtosecond laser ablation in glass for the inertial separation of microparticles, *Micromachines*, Vol. 9, No. 4, pp. 171, 2018.
[56] S. Ghadami, R. Kowsari-Esfahan, M. S. Saidi, K. Firoozbakhsh, Spiral microchannel with stair-like cross section for size-based particle separation, *Microfluidics and Nanofluidics*, Vol. 21, pp. 1-10, 2017.
[57] L.-L. Fan, Y. Han, X.-K. He, L. Zhao, J. Zhe, High-throughput, single-stream microparticle focusing using a microchannel with asymmetric sharp corners, *Microfluidics and nanofluidics*, Vol. 17, pp. 639-646, 2014.
[58] N. Nivedita, I. Papautsky, Continuous separation of blood cells in spiral microfluidic devices, *Biomicrofluidics*, Vol. 7, No. 5, 2013.
[59] A. Mihandoust, S. Razavi Bazaz, N. Maleki-Jirsaraei, M. Alizadeh, R. A. Taylor, M. Ebrahimi Warkiani, High-throughput particle concentration using complex cross-section microchannels, *Micromachines*, Vol. 11, No. 4, pp. 440, 2020.
[60] S. Shen, C. Tian, T. Li, J. Xu, S.-W. Chen, Q. Tu, M.-S. Yuan, W. Liu, J. Wang, Spiral microchannel with ordered micro-obstacles for continuous and highly-efficient particle separation, *Lab on a Chip*, Vol. 17, No. 21, pp. 3578-3591, 2017.
[61] Y. Gou, S. Zhang, C. Sun, P. Wang, Z. You, Y. Yalikun, Y. Tanaka, D. Ren, Sheathless inertial focusing chip combining a spiral channel with periodic expansion structures for efficient and stable particle sorting, *Analytical chemistry*, Vol. 92, No. 2, pp. 1833-1841, 2019.
[62] K. Erdem, V. E. Ahmadi, A. Kosar, L. Kuddusi, Differential sorting of microparticles using spiral microchannels with elliptic configurations, *Micromachines*, Vol. 11, No. 4, pp. 412, 2020.
[63] A. Gangadhar, S. A. Vanapalli, Inertial focusing of particles and cells in the microfluidic labyrinth device: Role of sharp turns, *Biomicrofluidics*, Vol. 16, No. 4, 2022.
[64] S. Ebrahimi, M. Alishiri, E. Pishbin, H. Afjoul, A. Shamloo, A curved expansion-contraction microfluidic structure for inertial based separation of circulating tumor cells from blood samples, *Journal of Chromatography A*, Vol. 1705, pp. 464200, 2023.
[65] S. C. Saha, I. Francis, T. Nassir, Computational Inertial Microfluidics: Optimal Design for Particle Separation, *Fluids*, Vol. 7, No. 9, pp. 308, 2022.

[66] T. Kim, H. Yoon, S. Nagrath, Optimization approach for inertial focusing and separation of cells in spiral microchannels, in *Proceeding of*, 26-30.

[67] S. Prakash, S. Kumar, Fabrication of microchannels: a review, *Proceedings of the Institution of Mechanical Engineers, Part B: Journal of Engineering Manufacture*, Vol. 229, No. 8, pp. 1273-1288, 2015.

[68] L.-J. Pan, J.-W. Tu, H.-T. Ma, Y.-J. Yang, Z.-Q. Tian, D.-W. Pang, Z.-L. Zhang, Controllable synthesis of nanocrystals in droplet reactors, *Lab on a Chip*, Vol. 18, No. 1, pp. 41-56, 2018.

[69] A. Olanrewaju, M. Beaugrand, M. Yafia, D. Juncker, Capillary microfluidics in microchannels: from microfluidic networks to capillaric circuits, *Lab on a Chip*, Vol. 18, No. 16, pp. 2323-2347, 2018.

[70] D. Sticker, R. Geczy, U. O. Hafeli, J. P. Kutter, Thiol–ene based polymers as versatile materials for microfluidic devices for life sciences applications, *ACS applied materials & interfaces*, Vol. 12, No. 9, pp. 10080-10095, 2020.

[71] A. Shakeri, N. A. Jarad, A. Leung, L. Soleymani, T. F. Didar, Biofunctionalization of glass-and paper-based microfluidic devices: a review, *Advanced Materials Interfaces*, Vol. 6, No. 19, pp. 1900940, 2019.

[72] A.-G. Niculescu, C. Chircov, A. C. Bîrcă, A. M. Grumezescu, Fabrication and applications of microfluidic devices: A review, *International Journal of Molecular Sciences*, Vol. 22, No. 4, pp. 2011, 2021.

[73] V. Sebastián Cabeza, *Advances in microfluidics-New applications in biology, energy, and materials sciences. Chap 17: High and Efficient Production of Nanomaterials by Microfluidic Reactor Approaches*, 9535127853, IntechOpen, pp. 2016.

[74] A. Singh, C. K. Malek, S. K. Kulkarni, Development in microreactor technology for nanoparticle synthesis, *International Journal of Nanoscience*, Vol. 9, No. 01n02, pp. 93-112, 2010.

[75] M. James, R. A. Revia, Z. Stephen, M. Zhang, Microfluidic synthesis of iron oxide nanoparticles, *Nanomaterials*, Vol. 10, No. 11, pp. 2113, 2020.

[76] K. Ren, J. Zhou, H. Wu, Materials for microfluidic chip fabrication, *Accounts of chemical research*, Vol. 46, No. 11, pp. 2396-2406, 2013.

[77] J. B. Nielsen, R. L. Hanson, H. M. Almughamsi, C. Pang, T. R. Fish, A. T. Woolley, Microfluidics: innovations in materials and their fabrication and functionalization, *Analytical chemistry*, Vol. 92, No. 1, pp. 150-168, 2019.

[78] C. Rivet, H. Lee, A. Hirsch, S. Hamilton, H. Lu, Microfluidics for medical diagnostics and biosensors, *Chemical Engineering Science*, Vol. 66, No. 7, pp. 1490-1507, 2011.

[79] S. B. Campbell, Q. Wu, J. Yazbeck, C. Liu, S. Okhovatian, M. Radisic, Beyond polydimethylsiloxane: alternative materials for fabrication of organ-on-a-chip devices and microphysiological systems, *ACS biomaterials science & engineering*, Vol. 7, No. 7, pp. 2880-2899, 2020.

[80] F. Kotz, M. Mader, N. Dellen, P. Risch, A. Kick, D. Helmer, B. E. Rapp, Fused deposition modeling of microfluidic chips in polymethylmethacrylate, *Micromachines*, Vol. 11, No. 9, pp. 873, 2020.

[81] P. Sengupta, K. Khanra, A. R. Chowdhury, P. Datta, *Lab-on-a-chip sensing devices for biomedical applications*, in: *Bioelectronics and medical devices*, Eds., pp. 47-95: Elsevier, 2019.

[82] M. A. Mofazzal Jahromi, A. Abdoli, M. Rahmanian, H. Bardania, M. Bayandori, S. M. Moosavi Basri, A. Kalbasi, A. R. Aref, M. Karimi, M. R. Hamblin, Microfluidic brain-on-a-chip: perspectives for mimicking neural system disorders, *Molecular neurobiology*, Vol. 56, pp. 8489-8512, 2019.

[83] J. Deng, W. Wei, Z. Chen, B. Lin, W. Zhao, Y. Luo, X. Zhang, Engineered liver-on-a-chip platform to mimic liver functions and its biomedical applications: A review, *Micromachines*, Vol. 10, No. 10, pp. 676, 2019.

[84] S. P. Kojic, G. M. Stojanovic, V. Radonic, Novel cost-effective microfluidic chip based on hybrid fabrication and its comprehensive characterization, *Sensors*, Vol. 19, No. 7, pp. 1719, 2019.

[85] Y. Gao, G. Stybayeva, A. Revzin, Fabrication of composite microfluidic devices for local control of oxygen tension in cell cultures, *Lab on a Chip*, Vol. 19, No. 2, pp. 306-315, 2019.

[86] J. Hwang, Y. H. Cho, M. S. Park, B. H. Kim, Microchannel fabrication on glass materials for microfluidic devices, *International Journal of Precision Engineering and Manufacturing*, Vol. 20, pp. 479-495, 2019.

[87] C. Iliescu, H. Taylor, M. Avram, J. Miao, S. Franssila, A practical guide for the fabrication of microfluidic devices using glass and silicon, *Biomicrofluidics*, Vol. 6, No. 1, 2012.

[88] C. A. Baker, R. Bulloch, M. G. Roper, Comparison of separation performance of laser-ablated and wet-etched microfluidic devices, *Analytical and bioanalytical chemistry*, Vol. 399, pp. 1473-1479, 2011.

[89] G. S. Fiorini, D. T. Chiu, Disposable microfluidic devices: fabrication, function, and application, *BioTechniques*, Vol. 38, No. 3, pp. 429-446, 2005.

[90] E. A. Waddell, Laser ablation as a fabrication technique for microfluidic devices, *Microfluidic Techniques: Reviews and Protocols*, pp. 27-38, 2006.

[91] V. Faustino, S. O. Catarino, R. Lima, G. Minas, Biomedical microfluidic devices by using low-cost fabrication techniques: A review, *Journal of biomechanics*, Vol. 49, No. 11, pp. 2280-2292, 2016.

[92] D. J. Guckenberger, T. E. De Groot, A. M. Wan, D. J. Beebe, E. W. Young, Micromilling: a method for ultra-rapid prototyping of plastic microfluidic devices, *Lab on a Chip*, Vol. 15, No. 11, pp. 2364-2378, 2015.

[93] A. L. Jáuregui, H. R. Siller, C. A. Rodríguez, A. Elías-Zúñiga, Evaluation of micromechanical manufacturing processes for microfluidic devices, *The International Journal of Advanced Manufacturing Technology*, Vol. 48, pp. 963-972, 2010.

[94] U. M. Attia, S. Marson, J. R. Alcock, Micro-injection moulding of polymer microfluidic devices, *Microfluidics and nanofluidics*, Vol. 7, pp. 1-28, 2009.

[95] B. K. Gale, A. R. Jafek, C. J. Lambert, B. L. Goenner, H. Moghimifam, U. C. Nze, S. K. Kamarapu, A review of current methods in microfluidic device fabrication and future commercialization prospects, *Inventions*, Vol. 3, No. 3, pp. 60, 2018.

[96] W. Su, B. S. Cook, Y. Fang, M. M. Tentzeris, Fully inkjet-printed microfluidics: a solution to low-cost rapid three-dimensional microfluidics fabrication with numerous electrical and sensing applications, *Scientific reports*, Vol. 6, No. 1, pp. 35111, 2016.

[97] P. Kim, K. W. Kwon, M. C. Park, S. H. Lee, S. M. Kim, K. Y. Suh, Soft lithography for microfluidics: a review, 2008.

[98] K. L. Wlodarczyk, R. M. Carter, A. Jahanbakhsh, A. A. Lopes, M. D. Mackenzie, R. R. Maier, D. P. Hand, M. M. Maroto-Valer, Rapid laser manufacturing of microfluidic devices from glass substrates, *Micromachines*, Vol. 9, No. 8, pp. 409, 2018.

[99] O. Skurtys, J. Aguilera, Applications of microfluidic devices in food engineering, *Food Biophysics*, Vol. 3, pp. 1-15, 2008.

[100] C. Dixon, J. Lamanna, A. R. Wheeler, Printed microfluidics, *Advanced Functional Materials*, Vol. 27, No. 11, pp. 1604824, 2017.

[101] Y. Alapan, M. N. Hasan, R. Shen, U. A. Gurkan, Three-dimensional printing based hybrid manufacturing of microfluidic devices, *Journal of Nanotechnology in Engineering and Medicine*, Vol. 6, No. 2, pp. 021007, 2015.